Article

Human Smc5/6 recognises transcription-generated positive DNA supercoils

Aurélie Diman [1,2] ✉, Gaël Panis[1,2,6], Cédric Castrogiovanni [3,4,6], Julien Prados [5], Bastien Baechler[1,2] & Michel Strubin[1,2]

Beyond its essential roles in ensuring faithful chromosome segregation and genomic stability, the human Smc5/6 complex acts as an antiviral factor. It binds to and impedes the transcription of extrachromosomal DNA templates; an ability which is lost upon integration of the DNA into the chromosome. How the complex distinguishes among different DNA templates is unknown. Here we show that, in human cells, Smc5/6 preferentially binds to circular rather than linear extrachromosomal DNA. We further demonstrate that the transcriptional process, per se, and particularly the accumulation of DNA secondary structures known to be substrates for topoisomerases, is responsible for Smc5/6 recruitment. More specifically, we find that in vivo Smc5/6 binds to positively supercoiled DNA. Those findings, in conjunction with our genome-wide Smc5/6 binding analysis showing that Smc5/6 localizes at few but highly transcribed chromosome loci, not only unveil a previously unforeseen role of Smc5/6 in DNA topology management during transcription but highlight the significance of sensing DNA topology as an antiviral defense mechanism.

The Smc5/6 complex belongs to the ring-shaped Structural Maintenance of Chromosomes (SMC) family complexes, which also includes the well-characterized cohesin (Smc1/3) and condensin (Smc2/4)[1]. These multi-subunit complexes, highly conserved in eukaryotes, are made of SMC heterodimers associated with a unique set of non-SMC-proteins (designated Nse1 to Nse4 in the case of Smc5/6). Powered by ATP, they entrap DNA molecules and contribute to chromosome architecture and dynamics[1,2]. While the roles of cohesin and condensin in fundamental chromosomal transactions have been clearly established, the cellular functions specific to Smc5/6 remain to be clarified[1,3]. The Smc5/6 complex has been linked to a wide range of cellular processes[4,5] such as DNA replication[6], DNA repair[7–10], telomere maintenance[11], and homologous recombination[12,13]. More recently, it has been identified as an antiviral factor targeting the hepatitis B virus (HBV)[14,15]. The binding of Smc5/6 to the circular HBV DNA genome impedes viral gene transcription and, thus, infection. To counteract the

restriction activity of the complex, HBV expresses HBx, a protein that targets Smc5/6 for ubiquitin-mediated proteasomal degradation[14,15]. Smc5/6 restriction activity is not limited to HBV. Several studies have documented the ability of Smc5/6 to inhibit the transcription and/or replication of other human pathogenic viruses. These include human papillomavirus (HPV)[16,17], herpes simplex (HSV-1)[18], Kaposi's sarcoma herpesvirus (KSHV)[19], unintegrated human immunodeficiency virus (HIV-1)[20], Epstein–Barr virus (EBV)[21] and polyomavirus (SV40)[22]. The hallmarks of these viruses are the expression of inhibitory proteins antagonizing the Smc5/6 restriction activity and the maintenance of their genomes as a chromatinized extrachromosomal circular DNA within the nucleus of the infected cell[14,16–22].

We previously reported that, as long as it remains extrachromosomal, the transcription of any reporter gene is silenced by Smc5/6. This occurs independently of the DNA sequence or the type of promoter used[14,23]. However, random chromosomal integration of the

[1]Department of Microbiology and Molecular Medicine, Faculty of Medicine, University of Geneva, Geneva 4, Switzerland. [2]Geneva Centre for Inflammation Research (GCIR), Faculty of Medicine, University of Geneva, Geneva 4, Switzerland. [3]Department of Cell Physiology and Metabolism, Faculty of Medicine, University of Geneva, Geneva 4, Switzerland. [4]Translational Research Centre in Onco-hematology, Faculty of Medicine, University of Geneva, Geneva 4, Switzerland. [5]Bioinformatics Support Platform, Faculty of Medicine, University of Geneva, Geneva 4, Switzerland. [6]These authors contributed equally: Gaël Panis, Cédric Castrogiovanni. ✉e-mail: aurelie.diman@gmail.com

reporter gene safeguards it from Smc5/6-mediated restriction[14,23]. As shown by a recent structure-function analysis of the complex, extra-chromosomal DNA (ecDNA) restriction is a property unique to Smc5/6, since neither cohesin nor condensin are involved[24]. The three-step restriction process involves the binding of Smc5/6 to ecDNA, their localization to Promyelocytic Leukemia Nuclear Bodies (PML-NBs), and subsequent transcriptional silencing through a yet unknown mechanism[24]. Since entrapment of ecDNA by Smc5/6 is a prerequisite to its restriction activity, we investigated and characterized the DNA substrate requirements for Smc5/6 binding in human cells.

In vitro studies revealed that both yeast and human Smc5/6 complexes possess an affinity for DNA tertiary structures featuring crossed DNA helices, such as plectonemes and catenated DNA templates[25,26]. These structures commonly arise during DNA replication and/or transcription processes and are typically resolved by topoisomerase enzymes (Top1 and Top2)[27]. In yeast cells, the accumulation of unresolved topological tension during DNA replication, caused by the depletion of Top2, leads to a significant increase in the binding of Smc5/6 to chromosomes[28].

Nevertheless, despite the intricate link observed between DNA supercoiling and Smc5/6 binding, the specific nature of the DNA structures recognized by the complex within cellular environment remains unclear.

Using several extrachromosomal reporter gene constructs in combination with chromatin immunoprecipitation (ChIP) in non-transformed immortalized human retina pigment epithelial cells (hTERT-RPE1), we show that ecDNA discrimination by Smc5/6 is not based on DNA uptakes route. Instead, the circular nature of the ecDNA is essential for Smc5/6 recognition since a linear extrachromosomal construct escapes both Smc5/6 binding and restriction. We also find that the transcriptional process itself, and not the RNA polymerase II transcription machinery, is implicated in Smc5/6 recruitment onto ecDNA. Modulation of DNA topoisomerase activity provides evidence that Smc5/6 binding depends on the accumulation of transcription-driven topological constraints. More specifically, by conducting additional topological characterization of the ecDNA, we find that in vivo, Smc5/6 binds to positively supercoiled DNA. Our comprehensive genome-wide analysis further confirms that the chromosomal association of Smc5/6 is also conditioned by transcription and the presence of positive DNA supercoils. Collectively, our data suggest a previously unsuspected role for Smc5/6 in the management of DNA superhelical stress generated during transcription and indicate that transcription-driven topological stress could be harnessed as a host defence mechanism against invaders.

Results

Smc5/6 restricts extrachromosomal DNA of both endogenous and exogenous origins

Since Smc5/6 restriction activity selectively operates on ecDNA templates introduced into cells either by transfection or viral transduction, we asked whether a chromosome-derived DNA circle would be detected and restricted by the complex[14,23]. For this purpose, we established a stable human cell line carrying an excisable chromosomal reporter construct that is not expressed when integrated into the chromosome (Fig. 1A). The construct was engineered such that upon Cre recombinase expression, using a self-excising lentiviral vector[29], the split *Gaussia luciferase* (*GLuc*) gene (*GLuc*-Nter and *GLuc*-Cter) flanked by two *LoxP* sites, embedded within a splice donor and acceptor sequences from an artificial intron, will form a circular ecDNA molecule. After transcription, the *LoxP*-containing intron is spliced out and a functional GLuc mRNA is formed. To monitor Cre-mediated excision, a green fluorescent reporter (*GFP*) gene was inserted at the 3′ end of the construct while the constitutive EF1α promoter lies at the 5′ end. Upon excision, this configuration brings the *GFP* gene under the control of the EF1α promoter. Visualization of GFP-positive cells

therefore provided a rapid and simple assessment of the recombination events (Fig. 1B). Excision efficiency, as well as extrachromosomal circle formation, were further quantified by real-time quantitative PCR (qPCR). Using three primer sets spanning the construct (Supplementary Fig. 1A), we showed that whereas the signal for the *GFP* coding region did not significantly change upon Cre-mediated excision (primer pair #G), as expected, the junction amplified by the primer pair #L almost completely disappeared. This coincided with the appearance of a new DNA junction, amplified by the primer pair #E, consistent with the generation of recombination-dependent extrachromosomal circles (Supplementary Fig. 1B). Measuring luciferase activity, we showed that *GLuc* gene expression from the excised extra-chromosomal circle increased in a Cre-dependent fashion following Smc5/6 complex degradation by HBx. Transduction in the same cells of an extrachromosomal reporter construct of exogenous origin expressing a *Cypridina luciferase* gene (*CLuc*) delivered thanks to an integrase-defective lentivirus (IND64A) showed a similar increase in luciferase activity but independently of Cre expression as expected (Fig. 1C). Similar results were obtained using two other cellular clones (Supplementary Fig. 1C). Overall, these results demonstrate that Smc5/6 restricts ecDNA independently of its origin.

Smc5/6 preferentially binds and restricts circular DNA templates

The preferential entrapment of circular DNA molecules, in vitro, by the purified budding yeast Smc5/6 complex[25,30], prompted us to ask whether a linear ecDNA would be detected by the human Smc5/6 complex in a cellular context. To answer this question, we modified an existing linear bacterial vector called pJazz®-OK[31] and made it suitable for reporter gene expression in mammalian cells. The *GLuc* gene under the control of a cytomegalovirus promoter (CMV) was cloned into the vector (Fig. 2A, upper panel). The covalently closed hairpin ends of the plasmid prevent its concatenation and its integration into the cellular chromosome. Taking advantage of two restriction enzyme sites (BssHII) present at both ends of the linear plasmid, we generated its circular counterpart, thereby allowing a direct comparison of the two constructs without any sequence bias (Fig. 2A, lower panel). Luciferase assays following transient transfection with either the circular or linear reporter constructs revealed that the circular DNA template was more strongly responsive to HBx compared to the linear template, which showed only weak stimulation (Fig. 2B). Furthermore, and as expected, despite similar transfection efficiency as measured by qPCR analysis (Supplementary Fig. 2), the basal expression level of the linear construct approximated those measured for the circular DNA template in the presence of HBx (Fig. 2B). We then examined whether the reduced stimulation of the linear reporter reflected a defect in Smc5/6 binding. ChIP experiments demonstrated, that indeed, Smc5/6 failed to stably associate with the linear ecDNA (Fig. 2C). Hence, linear ecDNA escapes Smc5/6 entrapment and silencing.

Smc5/6 binding to extrachromosomal DNA requires transcription but not RNA polymerase II

Chromosomal association of Smc5/6 has been reported to prevent accumulation of replication-induced DNA supercoiling[32]. Since the extrachromosomal reporter plasmids used in this study do not replicate, therefore excluding a role for replication in Smc5/6 binding, we investigate whether the topological stress induced by transcription promoted Smc5/6 loading onto ecDNA. We performed time-course experiments using two well-known transcription inhibitors. Cells were treated either with Actinomycin D (ACTD), which intercalates into the DNA helix thereby impeding the progression of the RNA polymerases[33], or with Triptolide (TPT), which inhibits the transcription initiation step and induces proteasomal-dependent degradation of the RNA polymerase II (RNAP II)[34]. Both inhibitory treatments suppressed RNA synthesis, as confirmed by the reduced incorporation of
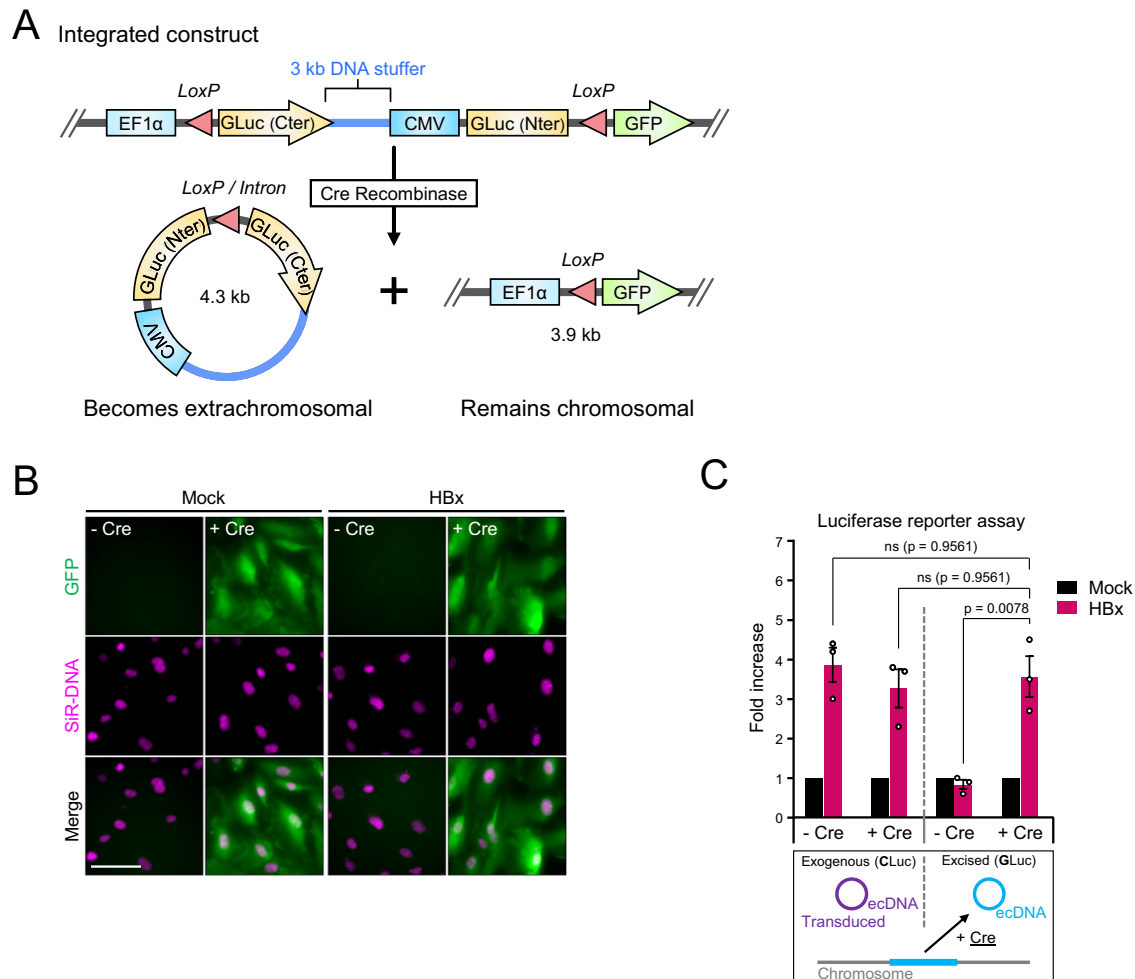
Fig. 1 | The origin of extrachromosomal DNA has no impact on the recognition and restriction by Smc5/6. A Schematic depiction of the genome-integrated construct used to generate extrachromosomal [Gluc^circle] and a chromosomally expressed *GFP* gene upon Cre/*loxP*-mediated excision. The yeast DNA stuffer is depicted in blue. **B** Live-cell representative images of Cre/*loxP*-mediated excision in hTERT-RPE1 cells containing the genomic excisable [Gluc^circle] construct were co-transduced with lentiviruses containing either no gene insert (Mock) or HBx, plus or minus the Cre recombinase. Nuclei were visualized with SiR-DNA. Scale bar, 100 μm. Data are representative of three independent experiments. **C** hTERT-RPE1 cells containing the genomic excisable [Gluc^circle] construct (excised ecDNA) were co-transduced with lentiviruses containing either no gene insert (Mock) or HBx, plus or minus the Cre recombinase, together with an integrase-defective lentiviral *Cypridina luciferase* (*CLuc*) reporter construct (exogenous ecDNA). The luciferase assay was performed 2 days post transduction. Luciferase activities are relative to their corresponding mock, which were set to 1. Data are means ± SEM of 3 independent experiments. Statistical analysis was performed using one-way ANOVA with Tukey's multiple comparisons. Source data are provided as a Source Data file.

the uridine analogue 5-ethynyluridine (EU), into newly transcribed RNA molecules (Supplementary Fig. 3A)[35]. Using anti-Smc5 and anti-Nse4 antibodies, we further confirmed by western blot analysis that none of the treatments alter the stability of the Smc5/6 complex, in contrast to what is observed upon HBx expression (Fig. 3A, B). ChIP experiments using HA-Smc6-expressing hTERT RPE-1 cells, showed that transcriptional arrest resulted in a specific dissociation of Smc5/6 from ecDNA while the level of histone H3 remained stable (Fig. 3C, D). In contrast, in DMSO-treated cells, the binding of Smc5/6 appears to be stable over time (Supplementary Fig. 3B).

Since Smc5/6 association depends on transcription, we explored if the nature of the RNA polymerase II machinery was important for the recruitment of the complex to ecDNA. An extrachromosomal construct carrying a GFP reporter gene under the control of the bacteriophage T7 RNA polymerase promoter was transduced in cells overexpressing a T7 RNA polymerase carrying a nuclear localisation signal (NLS-T7) (Fig. 3E, left panel). The nuclear localization of the T7 RNA polymerase was confirmed by immunofluorescence microscopy (Fig. 3E, right panel). Since it was previously reported that RNA pol II can drive transcription from a T7 promoter in mammalian cells[36], cells

were treated for 24 h with TPT prior to ChIP experiments. TPT is known to block RNA Pol II transcription while transcription driven by T7 RNA polymerase remains unaffected. Induction of transcription by the T7 RNA polymerase resulted in a twofold increase in the recruitment of the Smc5/6 complex to ecDNA (Fig. 3F–H). Altogether, those results highlight the notion that Smc5/6 binding is transcription-dependent but preclude that the recruitment occurs through interaction with the RNA pol II transcription machinery.

Smc5/6 detects transcription-induced topological structures that are substrates for topoisomerases

Several studies have found that both the human and yeast Smc5/6 complexes, have a marked preference for DNA tertiary structures such as plectonemes that arise upon accumulation of DNA supercoils[25,26]. Our data indicating that circular DNA, as well as transcription, are required for Smc5/6 binding (Figs. 2 and 3) prompted us to investigate the potential role of DNA topology in Smc5/6 recruitment to ecDNA. We hypothesized that Smc5/6 dissociation upon transcriptional arrest was due to the activity of topoisomerases (Top) which function to dissipate transcription-generated supercoils[27]. Concomitant knock-
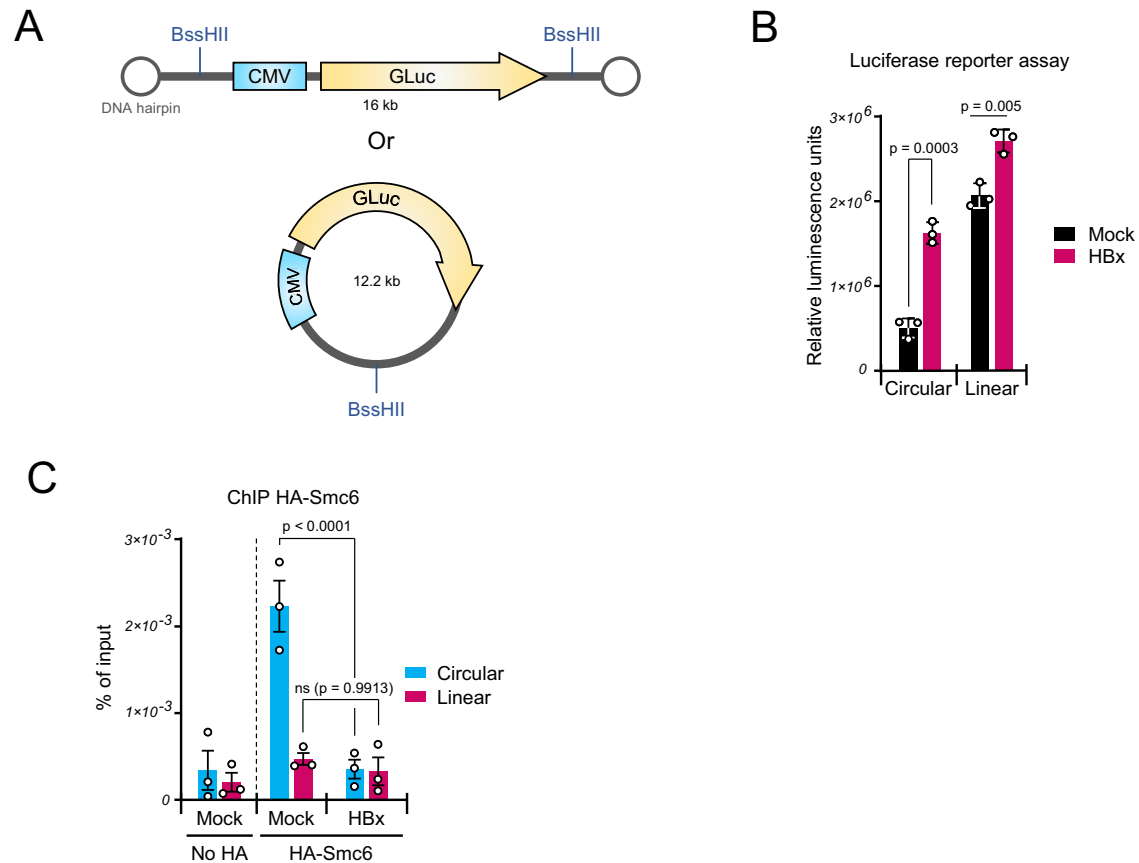
Fig. 2 | The binding and restriction activity of Smc5/6 are specific to circular DNA templates. A Schematic illustration of the linear pJAZZ®-derived vector with its terminal DNA hairpin loops, containing a mammalian expression cassette. The CMV promoter drives the expression of the *Gaussia Luciferase* gene. The BssHII restriction sites used to convert the linear vector into its circular form are also indicated. **B** hTERT-RPE1 cells over-expressing the HA-tagged version of Smc6 were transiently transfected with either a circular or a linear *Gaussia luciferase* reporter plasmid and then transduced with lentiviruses containing either no gene insert (Mock) or HBx. Luciferase activities were measured 2 days later and are presented as relative luminescence units (RLU). Data are means ± SEM of 3 independent experiments. Statistical analysis was performed using the two-sided Student's *t*-test. **C** hTERT-RPE1 cells (No HA) or hTERT-RPE1 cells over-expressing HA-tagged version of Smc6 were transiently transfected with either a circular or a linear *Gaussia luciferase* reporter plasmid and then transduced with lentiviruses containing either no gene insert (Mock) or HBx. Anti-HA ChIP was performed 2 days later. The data are expressed as a percentage of input. Data are means ± SEM of 3 independent experiments. Statistical analysis was performed using one-way ANOVA with Tukey's multiple comparisons. Source data are provided as a Source Data file.

downs of Top1, Top2A, and Top2B was performed to prevent any functional compensation of Top2A by Top2B[37,38]. Western blot analysis failed to detect Top2A in hTERT RPE-1 cells under our experimental conditions (Fig. 4A, C), but successful detection and knock-down validation was achieved in COLO320DM cells which exhibited higher Top2A expression levels (Supplementary Fig. 4). As expected, the simultaneous siRNA-mediated knock-down of Top1, Top2A and Top2B (Fig. 4A and Supplementary Fig. 4) in combination with transcription inhibition, prevented the dissociation of Smc5/6 from the ecDNA as shown by ChIP (Fig. 4B). Furthermore, c-Myc overexpression, which has been shown to stimulate Top1 and Top2 relaxation activities through the formation of the "topoisome" complex[39], led to Smc5/6 detachment, an event that could be counteracted by concomitant Top1, Top2A and Top2B siRNA-mediated depletion (Fig. 4C, D). Finally, to induce a targeted supercoil DNA relaxation of the ecDNA molecules, we overexpressed the myc-tagged DNA topoisomerase 1B from Vaccinia virus fused to a NLS (Myc-NLS-vTopIB) (Fig. 4E, F). This enzyme specifically recognizes the 5′-(C/T)CCTT-3′ DNA sequence[40,41] present at three different locations over the ecDNA. ChIP experiments performed in these cells revealed a reduction in Smc5/6 ecDNA binding (Fig. 4G) without an alteration in Smc5/6 complex stability (Fig. 4F). Altogether, these results point towards a DNA topology-dependent association of Smc5/6.

The genome-wide association of Smc5/6 depends on the DNA topological stress generated by transcription

Having shown that the accumulation of topological constraints due to transcription is responsible for the recruitment of Smc5/6 to ecDNAs, we asked if our results could recapitulate the Smc5/6 binding pattern on a genomic scale. Although Smc5/6 ChIP-sequencing (ChIP-seq) data are publicly available for *S.cerevisiae*[28,42], *Schizosaccharomyces pombe*[43], and *Mus.musculus*[44], to our knowledge, there is no such data reported for the human complex. Therefore, to gain more insights into the genome-wide Smc5/6 DNA-binding profile, we generated ChIP-seq data from HA-Smc6 and compared them to untagged Smc6 control cells. Our ChIP-seq results confirmed the ChIP-qPCR results with a 63-fold enrichment of reads mapping on the extrachromosomal *GLuc* ORF in the HA-Smc6 samples (Supplementary Fig. 5A). In addition, we identified a total of 41 binding sites for Smc5/6 throughout the human genome with a significant 2.5-fold enrichment compared to the no HA control cells (Fig. 5A DMSO and No HA). To test if the chromosomal association of Smc5/6 was also transcription-dependent, we performed ChIP-seq experiments following TPT treatment. In agreement with our observations previously made on ecDNA (Supplementary Fig. 5A), transcriptional arrest largely abrogated Smc5/6 binding on chromosomal DNA (Fig. 5A TPT). Surprisingly, the Red Fluorescent Protein reporter gene (*RFP*) present in the HA-Smc6 construct
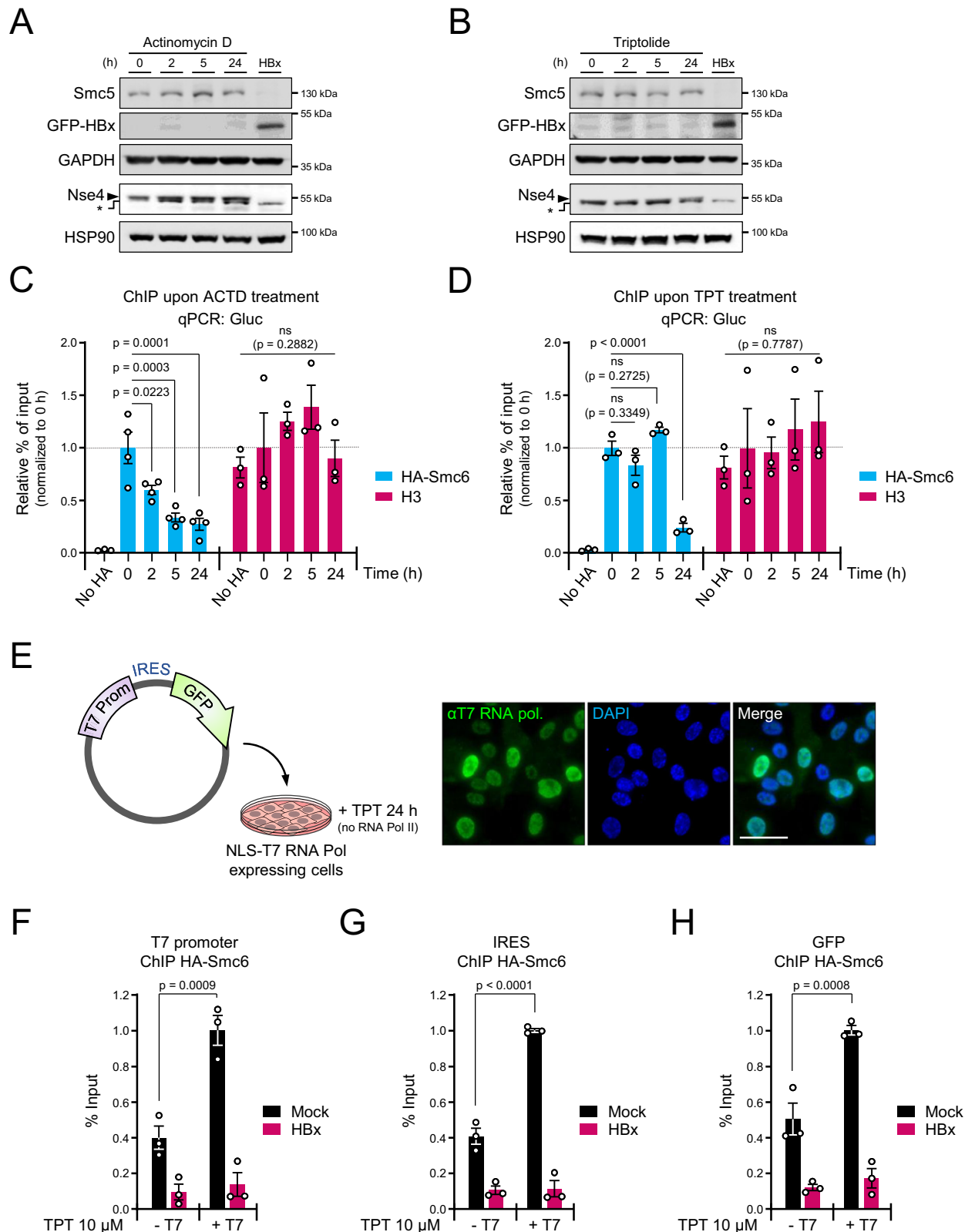
integrated into the chromosome also displayed Smc5/6 transcription-dependent binding (Supplementary Fig. 5B) but was not restricted by the complex, as previously reported[14]. To investigate in more detail the chromosomal relationship existing between Smc5/6 and the transcription process, we also performed ChIP-seq for RPB1, the largest RNAP II subunit[45], under the same experimental conditions. Heatmaps of the Smc5/6 bound-regions and RNAP II binding sites within 4 kb

around the Smc5/6 peak summit (Fig. 5A, B) revealed a colocalization between the Smc5/6 enriched-loci (78%) and the heavily bound RNAP II regions (Supplementary Fig. 5C). Comparison with publicly available RNA-seq profiles for RPE-1 cells[46], confirmed that those regions corresponded to hyperactive transcription sites (Supplementary Fig. 5D). Based on our previous observations, we decided to compare our Smc5/6-seq results with the published genome-wide mapping of

Fig. 3 | Recognition of extrachromosomal DNA by Smc5/6 is transcription-dependent but does not require RNA polymerase II. Western blots showing Smc5 and Nse4 levels in protein extracts of hTERT-RPE1 cells over-expressing HA-Smc6 treated for the indicated times with (**A**) 10 µg/ml Actinomycin D (ACTD) or (**B**) 10 µM Triptolide (TPT). Protein extract of GFP-tagged HBx expressing cells was used as a control for Smc5/6 complex degradation. *: Non-specific Nse4 band. Smc5 was used to assess the integrity of the Smc5/6 complex because only a small fraction of the overexpressed HA-Smc6 is assembled into the Smc5/6 complex that binds DNA and is consequently degraded by HBx[14,24]. hTERT-RPE1 cells (No HA) or HA-Smc6 hTERT-RPE1 cells transduced with an integrase-defective lentiviral luciferase reporter construct and treated with (**C**) ACTD or (**D**) TPT for the indicated times before anti-HA ChIP experiment (blues bars) or anti-H3 (pink bars). qPCR primers amplified the extrachromosomal *Gluc*. Data are expressed as a percentage relative to the input normalized to their corresponding 0 h time point set to 1 and are means ± SEM of 3 independent experiments. Statistical analysis was performed using one-way ANOVA with Tukey's multiple comparisons. **E** Experimental design depiction (left panel). Immunofluorescence staining of HA-Smc6 hTERT-RPE1 cells expressing T7 RNA polymerase with a nuclear localization signal (NLS) (right panel). Nuclei were stained with DAPI. Scale bar, 50 µm. **F**–**H** HA-Smc6 hTERT-RPE1 cells expressing or not the T7 RNA pol, co-transduced with lentiviruses containing either no gene insert (Mock) or HBx, together with an integrase-defective lentiviral construct carrying a *GFP* gene controlled by a T7 promoter and an IRES (Internal Ribosome Entry Site). Cells were treated with 10 µM Triptolide (TPT) for 24 h prior to anti-HA ChIP experiments. Three extrachromosomal regions - T7 promoter (**F**), IRES (**G**), GFP (**H**) - were tested and compared to their respective minus T7 RNA pol values. Data are expressed as a percentage relative to the input and are means ± SEM of 3 independent experiments. Statistical analysis was performed using one-way ANOVA with Tukey's multiple comparisons. Source data are provided as a Source Data file.

Top1[47] and Top2 activity[48]. We found that the Smc5/6 bound-regions overlapped with the Top1/Top2 bound loci along the transcription units, suggesting the presence of DNA supercoils at those loci (Fig. 5C). Interestingly, careful analysis of the Smc5/6 bound-regions identified a statistically significant enrichment of Smc5/6 downstream of the highly transcribe genes as exemplified by the depicted genomic regions (Fig. 5C). Altogether, these results suggest that the chromosomal binding of Smc5/6 could depend on DNA topological stress generated during transcription and accumulating at the 3'ends of highly transcribed genes.

Smc5/6 associates with positive DNA supercoils in human cells

To gain further insights into the chirality of DNA supercoiling recognized by Smc5/6 in vivo, we analyzed the topology of circular DNA extracted from human cells using two-dimensional (2D) gel electrophoresis followed by Southern blotting and hybridization with a specific radiolabelled DNA probe (Supplementary Table 3). By comparing the migration patterns of samples run in parallel on gels in the absence or in the presence of chloroquine, it becomes possible to distinguish between positively and negatively supercoiled DNA[49,50]. Chloroquine intercalates into DNA, altering the supercoil density and electrophoretic mobility of circular DNA molecules. When exposed to chloroquine, a circular DNA that is initially negatively supercoiled will lose superhelicity, leading to a decrease in its mobility. In contrast, a DNA circle that is already positively supercoiled will acquire further positive superhelical turns, resulting in increased compaction and faster migration through the gel[49]. To help us in the interpretation and identification of the different topological forms adopted in vivo by a covalently closed circular DNA, we conducted a comparative analysis between the topological profiles of extrachromosomal circular DNA recovered from cells and a similar DNA circle generated in vitro, which is known to be negatively supercoiled (Fig. 6A panel 1 and 2)[51]. As illustrated in Fig. 6A panel 3, the migration pattern of the DNA molecules retrieved from cells, located at the lower right end of the 2D gel arc, suggested that in vivo DNA circles consist in two distinct populations of supercoiled DNA molecules (Fig. 6A panel 3 red triangle and blue line). The increase in electrophoretic mobility (Fig. 6A panel 4) observed in the presence of chloroquine indicates that both DNA populations are positively supercoiled, with the upper one (red triangle) being slightly less positive than the lower one (blue line). Interestingly, while intermediate negatively supercoiled topoisomers are observed for the in vitro generated circles (Fig. 6A panel 2), no intermediate topoisomers were seen for the DNA circles retrieved from cells (Fig. 6A panel 4). This suggests a high intracellular level of superhelical density for these molecules indicating they could be hyperpositively supercoiled. These findings strongly indicate that, in vivo, the circular DNA molecules recognized by Smc5/6 are predominantly positively supercoiled.

To examine the genome-wide relationship between Smc5/6 binding and positive DNA supercoiling in human cells, we performed a GapR-seq analysis by expressing GapR-HA at either low or high level in hTERT RPE-1 cells (Supplementary Fig. 6A). GapR, a bacterial nucleoid-associated protein from *Caulobacter crescentus*, has been shown to preferentially bind overtwisted DNA generated during transcription, not only in bacteria[52,53] but also in yeast[53], making it an in vivo sensor for positively supercoiled DNA[53]. The comparison of the heatmap generated for RNA Pol II bound loci, sorted by fold enrichment (from highest to lowest), alongside the GapR peaks identified in cells expressing either a low or a high level of GapR, reveals a positive correlation between RNA Pol II and GapR enrichment at those loci (Supplementary Fig. 6B). This suggests that in human cells, as it was reported in both yeast and bacteria[53], GapR occupancy is strongly associated with transcriptional levels and its binding indicates the presence of transcription-generated positive DNA supercoiling. We generated heatmaps of GapR enrichment surrounding the Smc5/6-bound regions, and found that, about 50% of all Smc5/6 peaks in cells with high GapR expression and 12% in cells with low GapR expression, had significant neighboring GapR enrichment (1.5-fold with $a \leq 0,05$ q-value) within 4 kb (Fig. 6B). These observations suggest the presence of positive supercoiled DNA in the vicinity of the Smc5/6 bound-regions. Additionally, compared to no HA control cells, a threefold to fourfold enrichment of reads mapping on the extrachromosomal *GLuc* in the GapR-HA samples was observed (Supplementary Fig. 6C). Collectively, these findings strongly indicate that in vivo, Smc5/6 recognizes positive supercoils both on chromosomal and ecDNA.

Discussion

The unexpected discovery that Smc5/6, besides its crucial role in maintaining genome stability, also acts as a transcriptional repressor that specifically targets ecDNA, raises an important question[14,15,23]: How can a host genome architectural factor distinguish between chromosomal and ecDNA inside the nucleus? As a first step towards elucidating the mechanism that makes Smc5/6-mediated transcriptional suppression specific to ecDNA, we characterized the DNA requirements for Smc5/6 binding. Using an excisable reporter construct, we showed that the Smc5/6 complex does not discriminate ecDNA molecules based on their chromosomal or non-chromosomal origin. Since Smc5/6 possesses the ability to restrict chromosome-derived DNA circle, it suggests that Smc5/6 recognition is not influenced by specific chromosomal DNA features such as specific DNA modifications. This aligns with recent findings showing that Smc5/6 has the ability to restrict EBV, HPV, and KSHV. These viruses have ecDNA genomes that replicate simultaneously with the host genome, thus being packaged with chromatin resembling that of the host chromosome[16,17,19,21]. Instead, it likely depends on certain structural characteristics of the DNA it interacts with. Indeed, we have shown that Smc5/6 preferentially targets circular ecDNA molecules while linear
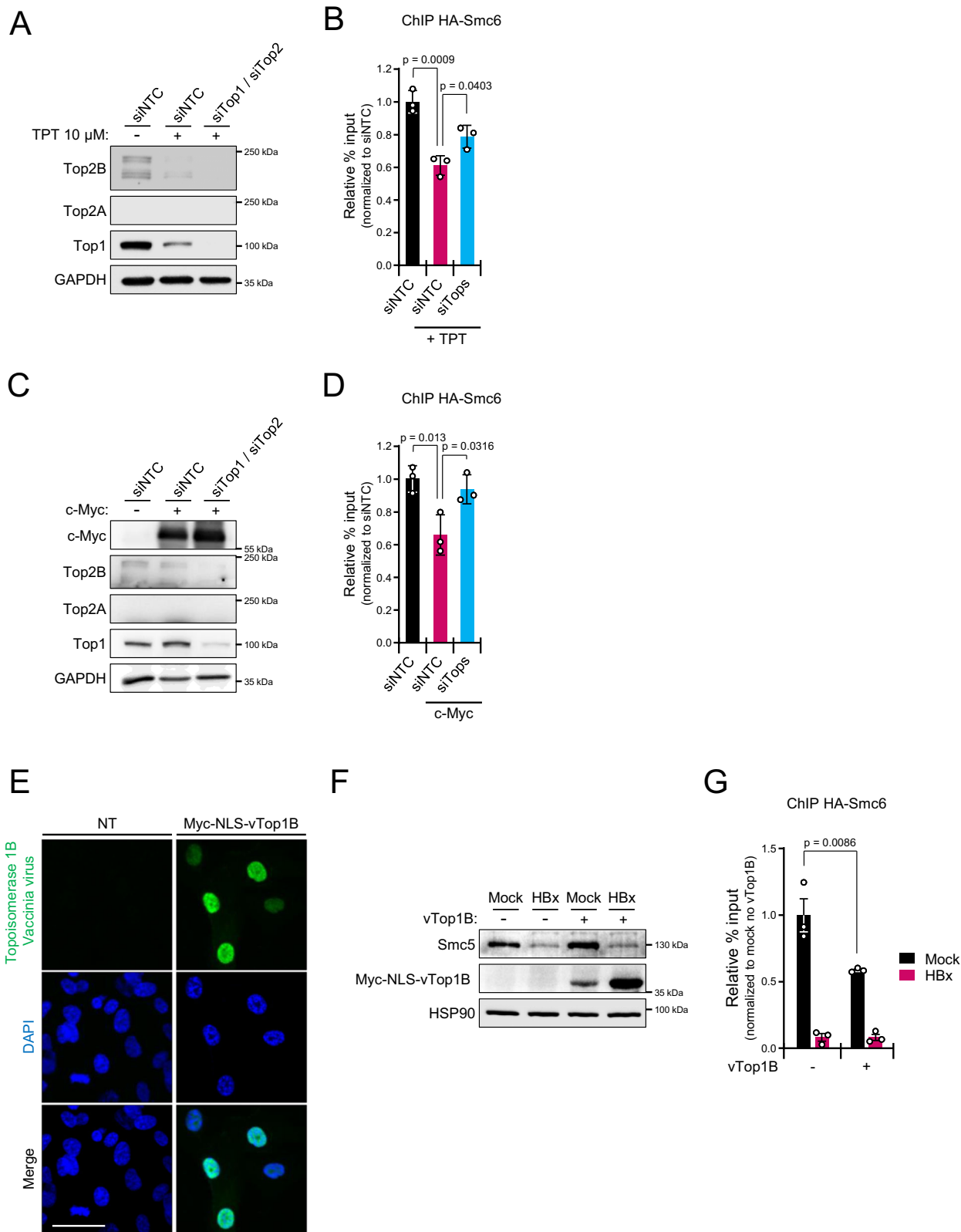
ecDNA escapes Smc5/6 topological entrapment. These results are consistent with in vitro pull-down experiments demonstrating the salt-stable binding of the budding yeast Smc5/6 complex to circular, but not linear, DNA templates[30,54]. We hypothesized that the helical topology of DNA could be a critical determinant for Smc5/6 loading. A linear DNA molecule can dissipate topological stress simply by spinning around its own helical axis, whereas a covalently closed circular

DNA accumulates high levels of superhelical tension, building-up higher-order DNA structures such as plectonemes[55]. The transcribing RNA polymerase is a potent generator of DNA supercoils[56]. According to the twin supercoiling domain model, the torque imposed on the DNA continuously generates negative supercoils behind and positive supercoils ahead of the RNA polymerase[57]. Our results showing that the transcription process itself, rather than components of the RNA

Fig. 4 | Smc5/6 recognizes topological structures arising during transcription which are substrates for topoisomerases. HA-Smc6-expressing hTERT RPE-1 cells transduced with an integrase-defective lentiviral luciferase reporter construct transfected with non-targeting control siRNA (siNTC) or with siRNAs against topoisomerase 1 (siTop1) and topoisomerases 2A and 2B (siTop2) before treatment or not with 10 µM Triptolide (TPT) prior to (**A**) Western blot analysis and (**B**) ChIP experiments using anti-HA (siTops: siTop1 and siTop2). ChiP data are expressed as a percentage relative to the input normalized to the siNTC alone (or not treated with TPT), which was set to 1. Data are means ± SEM of 3 independent experiments. Statistical analysis was performed using one-way ANOVA with Tukey's multiple comparisons. **C**, **D** HA-Smc6-expressing hTERT RPE-1 cells co-transduced with lentiviruses containing either no gene insert (Mock) or encoding the *c-Myc* gene, together with an integrase-defective lentiviral luciferase reporter construct were transfected with siNTC or with siTop1 and siTop2. **C** Western blot and (**D**) ChIP using anti-HA were performed after 3 days (siTops: siTop1 and siTop2). The ChiP data are expressed as a percentage relative to the input normalized to the siNTC

alone, which was set to 1. Data are means ± SEM of 3 independent experiments. Statistical analysis was performed using one-way ANOVA with Tukey's multiple comparisons. **E** Immunofluorescence staining of HA-Smc6-expressing hTERT RPE-1 cells transduced or not (NT) with lentiviruses encoding a N-terminal 3xMyc-tag-NLS topoisomerase 1B from vaccinia virus (Myc-NLS-vTop1B). Nuclei were stained with DAPI. Scale bar, 50 µm. **F**, **G** HA-Smc6-expressing hTERT RPE-1 cells expressing or not Myc-NLS-vTop1B, transduced with an integrase-defective lentiviral luciferase reporter, were co-transduced with lentiviruses containing either no gene insert (Mock) or HBx. **F** Western blots using an anti-Myc confirmed the expression of Myc-NLS-vTop1B with no impact on Smc5/6 complex integrity as demonstrated by Smc5 protein levels. **G** ChIP with anti-HA were performed after 3 days. ChiP data are expressed as a percentage relative to the input normalized to no Topo1V mock, which was set to 1. Data are means ± SEM of 3 independent experiments. Statistical analysis was performed using one-way ANOVA with Tukey's multiple comparisons. Source data are provided as a Source Data file.

pol II transcription machinery, is responsible for Smc5/6 recruitment onto circular ecDNA suggests an involvement of the DNA superhelicity. Supporting the DNA topology-dependent association of Smc5/6, we show that preventing supercoil removal by knocking down cellular topoisomerases counteracts the detachment of Smc5/6 observed after transcriptional switch-off. These findings were corroborated by the demonstration that Smc5/6 affinity for circular ecDNA was decreased upon reduction of their supercoil levels induced either by stimulation of endogenous topoisomerase activity or by overexpression of a viral topoisomerase. Biophysical experiments conducted with the purified complex showed the preferential binding of Smc5/6 to structured DNA such as plectonemic substrates[25,26]. However, discrepancies persist among these in vitro studies. So far, they have encountered challenges in establishing a clear preference of Smc5/6 for DNA supercoils based on their chirality[25,26]. To date, due to the technical limitations in monitoring DNA supercoiling in vivo, the DNA characteristics required for Smc5/6 recruitment have only been inferred based on the genomic loci where Smc5/6 binding occurs[28,58]. Here, by cross-comparing the ChIP-seq data for Smc5/6 and GapR, a bacterial protein proposed to probe DNA-positive supercoiling in vivo[52,53], we observed that GapR localized in the vicinity of Smc5/6 binding sites. This correlation suggests that positive DNA supercoiling is present within these regions, as previously suggested for yeast cells[53,58]. Using DNA topology assay, we directly assessed the supercoiling state of the ecDNA bound by Smc5/6 and showed that in vivo, Smc5/6 preferentially binds to supercoiled DNA with positive handedness (Fig. 6A). Our 2D-gel analysis also revealed the presence of a second population of DNA circles displaying a reduced level of positive supercoiling. This reduced level of positive supercoiling might find its explanation in a recent study which demonstrates that, under specific conditions, the yeast Smc5/6 complex can negatively twist DNA during loop extrusion[59,60]. It remains to be determined whether these observations also apply to the human complex. Additionally, the lack of intermediate topoisomers for DNA circles isolated from cells, in contrast to those generated in vitro, implies a high intracellular level of superhelical density. Based on previous findings[24], we hypothesized that ecDNAs could be confined in a condensed state within subnuclear compartments, such as PML-NBs, which have previously been shown to be essential for Smc5/6-mediated extrachromosomal restriction[61]. This would align with previous studies correlating Smc5/6 binding to chromatin compaction, leading to the formation of a repressive chromatin structure that ultimately silences extrachromosomal gene expression[20,25,26].

Unexpectedly, our ChIP-seq analyses revealed a genome-wide interdependency between topological stress accumulation due to transcription and Smc5/6 binding at multiple, but nevertheless a restricted number of DNA loci. This suggests that the Smc5/6 complex is required in specific transcriptional scenarios because not all the

transcribe loci were bound by the complex, but only those with elevated transcriptional levels. Therefore, we envision a model (Fig. 7) in which the very high transcriptional output of certain genes leads to an abnormally high level of DNA supercoil accumulation, generating DNA secondary structures that ultimately result in the recruitment of the Smc5/6 complex. Moreover, since Smc5/6 has been proposed to not only bind but also stabilize DNA plectonemes[25], we advance a scenario in which Smc5/6 would trap and gather the excessive buildup of positive supercoils generated in front of the transcription machinery. The Smc5/6-mediated local plectoneme containment could either prevent supercoil propagation, which could inhibit subsequent transcription at neighboring genes, or promote the effective interaction between the DNA secondary structures and the topoisomerases or a combination of both. Collectively, our data suggest that by sensing and monitoring the levels of DNA torque in vivo, Smc5/6 might act as a topological insulator inhibiting the diffusion of transcription-induced positive supercoils. Since in yeast cells, Smc5/6 has been recently proposed to organize 3D positive supercoiled DNA loops generated by transcription[58], it would be interesting to investigate in human cells the impact of Smc5/6 depletion on long-range DNA interactions as well as global genome transcription. Moreover, given that Smc5/6 binding requirements appear to be similar for chromosomal and ecDNA, uncovering the molecular events that drive the Smc5/6-mediated transcriptional repression towards ecDNA may provide insight into whether the Smc5/6 complex's restriction activity differs from its role in regulating chromosomal DNA transcription, or if they are both interconnected facets of the same process. Future studies should aim to address the interplay between DNA supercoils, Smc5/6, and topoisomerases in order to fully elucidate the functions of the Smc5/6 complex in transcription regulation in human cells.

In summary, our findings identified an unexpected function of the Smc5/6 complex in managing DNA superhelical stress arising from transcription, along with its preferential binding to positive DNA supercoils in human cells. Moreover, these results unveiled a previously unsuspected role of DNA topology sensing as a key defense mechanism against viral and other extrachromosomal genetic threats.

Methods
Cell culture
The hTERT-RPE1 (non-transformed immortalized human retina pigment epithelial cells) (ATCC; CRL-4000) (kind gift from P. Meraldi), human embryonic kidney cell line HEK 293T/17 (ATCC; CRL-11268), human adenocarcinoma epithelial cells HeLa (ATCC; CCL-2) and the human colon cancer carcinoma COLO320DM (kind gift from H. Y. Chang) cells and their derivatives, were grown at 37 °C under 5% CO_2 in high glucose DMEM (Gibco; 41966029) supplemented with 10% FBS (Gibco; 10270-106), 1% penicillin/streptomycin (Sigma; P0781-100), 2 mM L-glutamine (25030024), 1 mM sodium pyruvate (11360070),
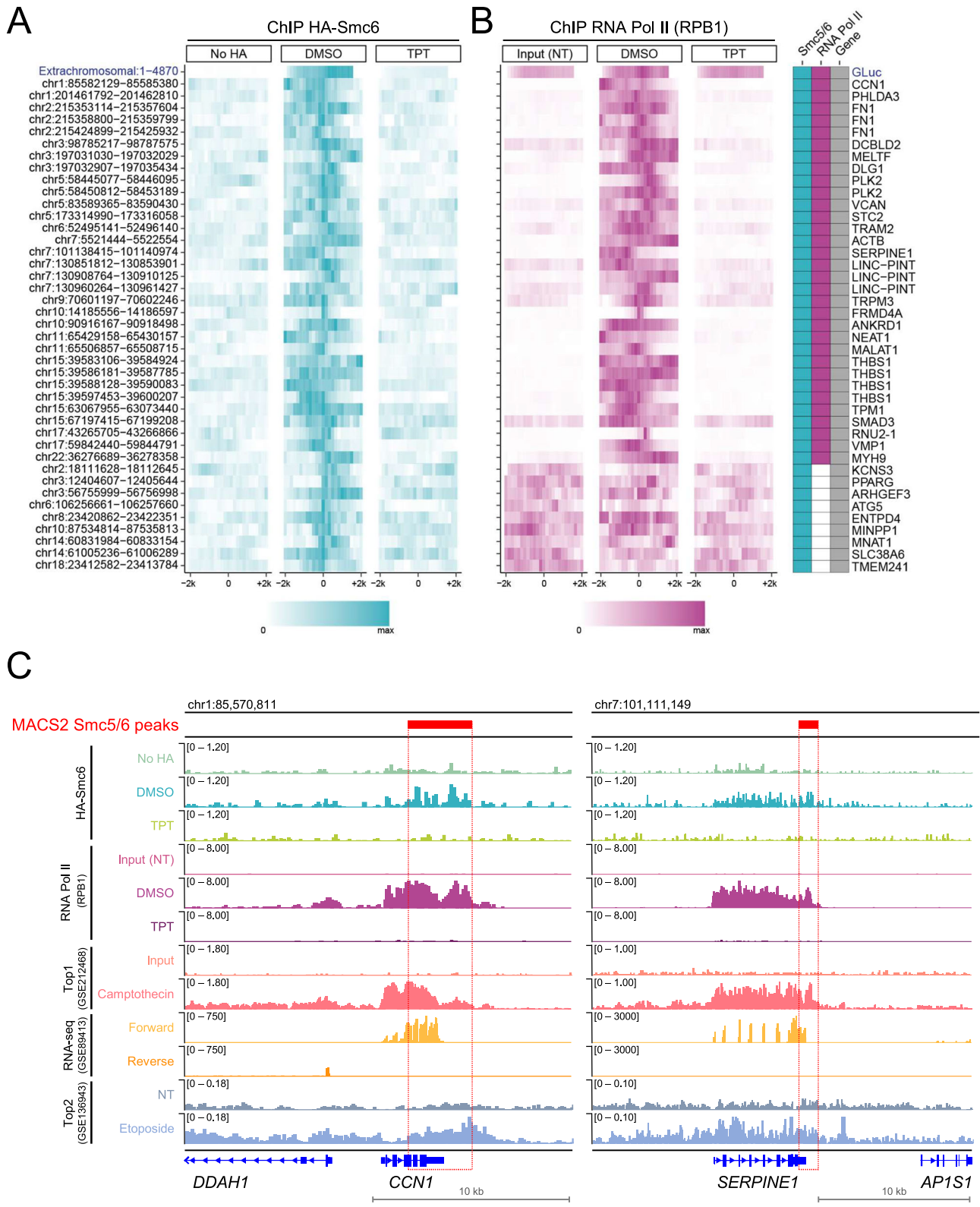
To generate the hTERT-RPE1 cell line over-expressing the HA-tagged version of Smc6, hTERT-RPE1 cells (ATCC; CRL-4000) were transduced with pCDH-CMV-3xHA-Smc6-EF1α-RFP lentiviral vector.

One month post-transduction, positive RFP cells were fluorescence-activated cell sorted, and used for further experiments.

To obtain the hTERT-RPE1 clones with a chromosomally integrated excisable [GLuc^{circle}] construct, hTERT-RPE1 cells (ATCC; CRL-4000) were transduced with a lentiviral vector (System Biosciences

Fig. 5 | The chromosomal association of Smc5/6 depends on DNA topological stress induced during transcription. A Heatmaps of the ChIP-seq read depth around 41 identified Smc5/6 complex binding sites: in hTERT-RPE1 cells (No HA) (left panel); hTERT-RPE1 cells over-expressing a HA-tagged version of Smc6 treated either with DMSO (middle panel); and 10 μM Triptolide (TPT) (right panel) before HA-ChIP. Cells were transduced with an integrase-defective lentiviral luciferase reporter construct (GLuc). Rows represent Smc5/6 binding sites ±2 kb around the peak summit, ordered by chromosome number and according to the presence or absence of RNA Pol II as determined by RPB1-ChIP-seq (**B**). Peaks statistically detected using MACS2 software analysis (2.5 fold enrichment, 0.05 *q*-value) are depicted. Color scale represents the ChIP-seq normalized read depth (RPM) row-scaled identically across the 3 samples, with mapped reads virtually resized to 1 kb-length and looking at each genomic position for the amount of overlap between forward- and reverse-stranded reads. **B** Heatmaps of RNA pol II ChIP-seq peaks in hTERT-RPE1 cells over-expressing a HA-tagged version of Smc6 treated either with DMSO (DMSO), 10 μM Triptolide (TPT) or the corresponding input (NT), before

RPB1-ChIP. Cells were transduced with an integrase-defective lentiviral luciferase reporter construct (GLuc). Rows: RNA pol II binding sites ±2 kb around the Smc5/6 peak summit, ordered by chromosome number and according to the presence or absence of RNA Pol II as determined by the RPB1-ChIP-seq results. Color scale represents the ChIP-seq normalized read depth (RPM) row-scaled identically across the 3 samples, with mapped reads virtually resized to 1 kb-length and looking at each genomic position for the amount of overlap between forward- and reverse-stranded reads. **C** Integrative Genomics Viewer (IGV) track screenshots from 2 representative genomic loci. Red line: Smc5/6 peaks location identified by MACS2. Tracks 1 to 3 (No Ha, DMSO, TPT) represent Smc5/6 ChIP-seq data for the corresponding samples, and tracks 4 to 6 (Input NT, DMSO, TPT) represent RNA pol II ChIP-seq data for the corresponding samples. The subsequent tracks, Top1 (GSE212468)[47], RNA-seq (GSE89413)[46], and Top2 (GSE136943)[48] depict publicly available data obtained for hTERT-RPE1 cells. Scales refer to the signal range in individual genome tracks.

#CD511B) encoding the excisable reporter construct (see details below). Two weeks post-transduction, single-cell clones were isolated by fluorescence-activated cell sorting in 96-well plates and expanded for two more weeks before screening. GLuc and GFP expression, before and after Cre recombinase expression, was used as screening criteria for each clone.

Transfections and treatments

siRNAs transfections were performed following the manufacturer's instructions for 72 h with 20 nM siRNAs using either siNTC or siTop1A, siTop2A, and siTop2B (Supplementary Table 1) (Horizon Discovery Ltd). Opti-MEM (ThermoFisher; 31985070) and Lipofectamine™ RNAiMAX (ThermoFisher; 13778150) were used.

For plasmid transfection, cells were transduced with the appropriate lentiviruses 24 h prior transfection and seeded at a density of 6×10^6 cells in a 10-cm dish. Cells were then reverse-transfected with 3 μg of reporter plasmid using Lipofectamine™ 2000 (ThermoFisher; 11668019) following the manufacturer's instructions. Analysis was performed 48 h later.

Actinomycin D (Enzo Life Sciences; BML-GR300-0005) and triptolide (Sigma; T3652) were used as indicated on the figures.

Plasmids and constructs

The lentiviral vector pWPT (Addgene #12255) was used to expressed either Mock (empty), GFP-HBx, or HBx alone[14]. pCDH-CMV-MCS-EF1-Puro (System Biosciences #CD510B) was used to express HBx in case of experiments done in presence of Cre recombinase. The Cre recombinase was expressed from the pLOX-CW-CRE (Addgene #12238). pCDH-CMV-MCS-EF1α-RFP lentiviral vector (System Biosciences #CD512B) was used to clone the human codon-optimized, chemically synthesized (System Biosciences) Smc6 gene sequence under the control of the CMV promoter which was further 3×HA-tagged. The secreted GLuc and the secreted Cypridina luciferase (CLuc) used as reporter were either expressed from pCDH-CMV-GLuc-EF1α-copGFP or pCDH-CMV-CLuc-EF1α-RFP, respectively, when delivered as ecDNA using an integrase-defective (D116A) lentiviral vector (System Biosciences #CD511B).

The excisable reporter construct was generated through several steps. A first segment containing the split GLuc gene sequence (GLuc-Nter aa 1 to 49 and Gluc-Cter aa 50 to 186), obtained from pCMV-GLuc(M60I) and separated by a chimeric intron (splicing donor and acceptor sequences both from pCI-neo, Promega; E1731) with an embedded inverted *LoxP* site, was amplified using several rounds of overlapping PCR with primers pairs (MS2330-MS2340), (MS2341-MS2333), (MS2342-MS2343), (MS2344-MS2345), (MS2346-MS2347), (MS2342-MS2347) and cloned into the BamHI and XbaI sites of pCMV-empty to generate pCMV-GLuc(Nter)-donnor-LoxP-acceptor-GLuc(Cter).

A second fragment containing the EF1α-*LoxP*-copGFP sequence was amplified using several rounds of overlapping PCR from pCDH-

CMV-GLuc-EF1α-copGFP with primers pairs (MS2414-MS2415), (MS2416-MS2417), (MS2414-MS2463) (MS2348-MS2417), and (MS2414-MS2417) and cloned into the SpeI and PstI sites of pCDH-CMV-GLuc-EF1α-copGFP to generate pCDH-EF1α-*LoxP*-copGFP.

A unique NotI restriction site was added in the *LoxP* site sequence to facilitate further cloning steps.

The *LoxP*-copGFP form pCDH-EF1α-*LoxP*-copGFP was cloned in the NotI and PstI sites from pCMV-GLuc(Nter)-donnor-*LoxP*-acceptor-GLuc(Cter) to generate pCMV-GLuc(Nter)-donnor-*LoxP*-copGFP.

In parallel a 3 kb DNA sequence from the budding yeast *MDN1* gene, later called DNA stuffer, was PCR amplified and cloned into the XbaI and MluI sites of pLVX-CMV-GLuc(M60I) to generate the pLVX-CMV-GLuc-DNAstuffer.

The *LoxP*-acceptor-GLuc(Cter) from pCMV-GLuc(Nter)-donnor-LoxP-acceptor-GLuc(Cter) was cloned in the NotI and XbaI sites of pLVX-CMV-GLuc-DNAstuffer. The GLuc(Nter)-donnor-*LoxP*-copGFP generated from pCMV-GLuc(Nter)-donnor-*LoxP*-copGFP was further cloned in the MluI and PstI sites from this newly created construct to generate pLVX-CMV-GLuc-*LoxP*-acceptor-GLuc(Cter)-DNA stuffer-CMV-GLuc(Nter)-donnor-*LoxP*-copGFP.

To generate the final lentiviral construct pCDH-EF1α-*LoxP*-acceptor-GLuc(Cter)-DNAstuffer-CMV-GLuc(Nter)-donnor-*LoxP*-copGFP, the *LoxP*-acceptor-GLuc(Cter)-DNAstuffer-CMV-GLuc(Nter)-donnor-*LoxP*-copGFP obtained after partial digestion of pLVX-CMV-GLuc-*LoxP*-acceptor-GLuc(Cter)-DNA stuffer-CMV-GLuc(Nter)-donnor-*LoxP*-copGFP was cloned in the NotI and PstI sites of pCDH-EF1α-*LoxP*-copGFP.

The linear pJazz mammalian expression vector was obtained by cloning the CMV-GLuc-EF1α-copGFP cassette from pCDH-CMV-GLuc-EF1α-copGFP into the SpeI and NotI sites of pJazz®-OK (kind gift from M. Brochet). Its circular counterpart was obtained after digestion with BssHII and self-ligation.

To generate the NLS-T7-polymerase lentiviral vector, the DNA fragment corresponding to the NLS-T7-polymerase sequence was PCR amplified using the primer pairs (5′-CGAACCCTTGGATCCGCCAC-CATG-3′ and 5′-GCCGCGGCCGCACCGGTAGGGATCG-3′) from the pcDNA3.4-T7pol plasmid (kind gift from G. Kudla)[62] and cloned into the BamHI and NotI sites of the pCDH-CMV-MCS-EF1α-RFP lentiviral vector (System Biosciences #CD512B). The T7 promoter-IRES-GFP reporter lentiviral construct was generated by PCR amplification of the corresponding DNA fragment from the pUC19-T7-pro-IRES-EGFP plasmid (kind gift from G. Kudla)[62] using the primer pairs (5′-CGGATCGATTGTAAAACGACGGCCAGTGAATTC-3′ and 5′-CGGTCGA CTTAAAGACAGGCCTTACTGGCTGAATAGA-3′) and cloned into the ClaI and SalI sites of the pCDH-CMV-GLuc-EF1α-copGFP lentiviral vector (System Biosciences #CD511B) from which the CMV promoter was previously removed.

To generate the c-Myc expression vector, the c-Myc sequence from the pCDH-Puro-cMyc plasmid (Addgene #46970) was cloned into
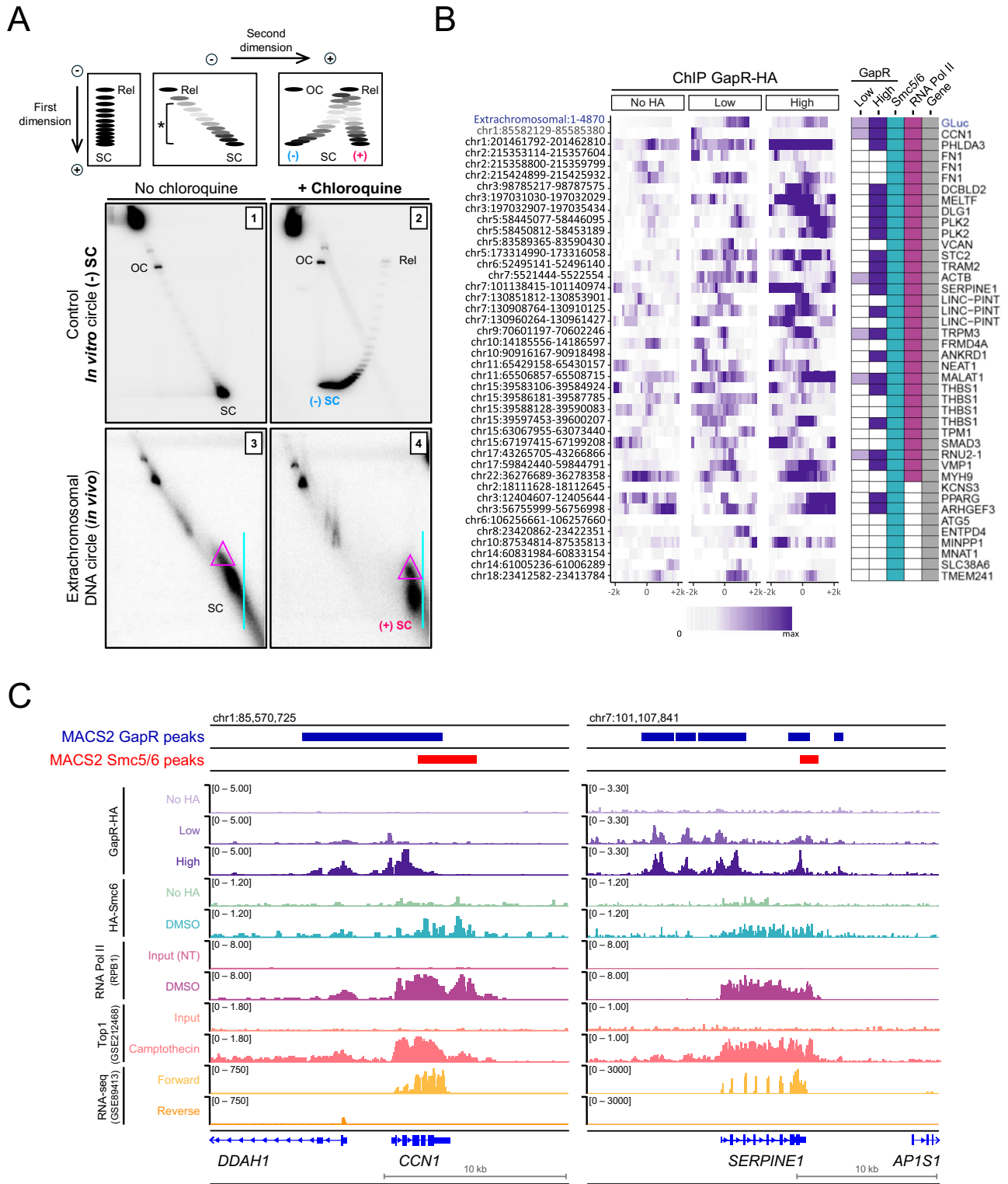
the XbaI and NotI sites of the pCDH-CMV-MCS-EF1α-RFP lentiviral vector (System Biosciences #CD512B).

The Myc-tagged DNA topoisomerase IB from vaccinia virus fused to a NLS (Myc-NLS-vTopIB) sequence was chemically synthesized and cloned in the sites XhoI and XbaI of the pLVX-CMV-MCS-PGK-Puro lentiviral vector (BioCat GmbH).

The GapR protein, tagged with HA (GapR-3xHA), derived from *Caulobacter crescentus*, was codon-optimized for expression in human cells. It was chemically synthesized and cloned into the EcoRI and BamHI sites of the pLVX-CMV-MCS-PGK-Puro lentiviral vector (BioCat GmbH).

All the primers used are listed in Supplementary Table 1. Phusion High-Fidelity DNA polymerase (Thermo Scientific; F530L) was used for all the PCR reactions. All the restriction enzymes and T4 DNA ligase were from NEB.

Lentivirus production and titration
Briefly, 4.5 × 10⁶ HEK 293T/17 cells were plated in a 10-cm dish and transiently transfected 16 h later using the calcium phosphate method with 15 µg lentiviral vector plasmid, 10 µg of packaging plasmid psPAX2 (Addgene plasmid #12260), and 5 µg of envelope plasmid

Fig. 6 | In human cells, Smc5/6 binds to positively supercoiled DNA. A Upper part: Schematic showing migration patterns in 2D gel electrophoresis of positively/negatively supercoiled circular DNA with/without chloroquine. Rel: relaxed, OC: open circular, *: topoisomer bands. Lower part: Southern blots of 2D gels on the control circles generated in vitro (panels 1 and 2) and on the circles recovered from cells (panels 3 and 4) with (panels 2 and 4) or without (panels 1 and 3) chloroquine. Blue line: main supercoiled population migration front. Red triangle: slightly less positively supercoiled population. **B** Heatmaps of GapR ChIP-seq peaks in hTERT-RPE1 cells No HA (left panel) or hTERT-RPE1 cells over-expressing a HA-tagged GapR at low (Low); and high levels (High). Cells were transduced with an integrase-defective lentiviral luciferase reporter construct (GLuc). Rows: GapR binding sites ±2 kb around the Smc5/6 peak summit, ordered by chromosome number according to the presence or absence of RNA Pol II as determined by the RPB1-ChIP-seq results. Peaks statistically detected using MACS2 software analysis (≥1.5-fold enrichment, ≤0.05 *q*-value) are indicated by a filled box on the right panel. The color scale represents the ChIP-seq normalized read depth (RPM) row-scaled identically across the 3 samples, with mapped reads virtually resized to 1 kb-length and looking at each genomic position for the amount of overlap between forward- and reverse-stranded reads. **C** Integrative Genomics Viewer (IGV) track screenshots from 2 representative genomic loci. Dark blue line: GapR peaks location identified by MACS2. Track 1 to 3 (No HA, Low GapR, High GapR) represent GapR ChIP-Seq data for the corresponding samples. Red line: Smc5/6 peaks location identified by MACS2. Tracks 4 to 5 (No HA, DMSO) represent Smc5/6 ChIP-seq data for the corresponding samples. Tracks 7 to 8 (Input NT, DMSO) represent RNA pol II ChIP-seq data for the corresponding samples. The subsequent tracks, Top1 (GSE212468)[47], RNA-seq (GSE89413)[46] depict publicly available data obtained for hTERT-RPE1 cells. Scales refer to the signal range in individual genome tracks. Source data are provided as a Source Data file.

pMD2G (Addgene plasmid #12259) to produce VSV-G pseudotyped recombinant lentiviruses. To produce integrase-defective lentiviruses, the plasmid p8.9NdSB (king gift from J. Luban) which encoded a catalytically inactive integrase point mutant (D116A) was used in replacement of the psPAX2. 8 h post transfection the culture medium was changed. Two days later, supernatants containing the viral particles were collected and filtered through PVDF 0.45 μm filters (Merck-Millipore; SLHV033RS) before storage at −80 °C. The titer of lentiviruses expressing GFP or RFP was estimated, by fluorescence-activated cell sorting analysis of GFP-positive or RFP-positive cells after infecting HeLa cells for 4 days with serially diluted viral supernatants.

Luciferase reporter gene assay
Luciferase activities were measured 2–3 days after reporter transfection or transduction. Briefly, 5 μL of cell culture supernatants were mixed with 50 μL of Luciferase assay buffer (100 mM NaCl, 35 mM EDTA, 0.1% Tween® 20, 300 mM sodium ascorbate in 1× phosphate-buffered saline) containing as substrate either: 4 μM coelenterazine (Biosynth AG; C-7001) in case of GLuc or 1 μM vargulin (NanoLight; 305) for CLuc. Luminescence was measured in triplicates in a 96-microplate luminometer (Glomax; Promega).

Western blotting
Cell lysis was performed in 2% sodium dodecyl sulfate (SDS) (Sigma; 71729) in water, and the lysates were denatured at 95 °C for 5 min. Protein concentrations were estimated using the Pierce™ BCA Protein Assay kit (Thermo Scientific; 23225). Equal amounts of proteins (30–50 μg) were separated on 8–18% SDS-PAGE gradient gels and electroblotted onto nitrocellulose membranes (Amersham; 10600003). The membranes were blocked in 5% (w/v) non-fat dry milk −PBST 0.1% [Phosphate-buffered saline (ThermoFisher; 14190094) supplemented with 0.1% Tween® 20 (Sigma; P1379)] for 1 h and incubated overnight with primary antibodies at 4 °C in 5% milk−PBST 0.1%. The membranes were then washed thrice with PBST 0.1% for 10 min, and incubated with secondary antibodies for 1 h at RT. The membranes were finally washed thrice with PBST 0.1% for 10 min. Detection was performed with SuperSignal West Pico PLUS chemiluminiscent substrate (Thermo Scientific; 34580) according to the manufacturer's protocol. Images were acquired with the ChemicDoc XRS luminescence imager from Bio-Rad. The primary and secondary antibodies used are listed in Supplementary Table 2.

ChIP and quantitative PCR
ChIP analysis was performed using chromatin extracted from about 5×10^6 HA-tagged Smc6 expressing hTERT-RPE1 or HA-tagged GapR-expressing hTERT-RPE1 (Low expression = single lentiviral transduction; High expression = double lentiviral transductions) cells cultured in a 10-cm diameter dish. Cells were harvested with trypsin-EDTA and collected by low-speed centrifugation $500 \times g$ for 5 min. Cells were rinsed once with PBS, resuspended in DMEM, and fixed with 1% formaldehyde (Sigma; 47608) for 10 min at RT before quenching with 330 mM glycine 5 min at RT and then 15 min on ice. After two further washes with ice-cold PBS, cells were resuspended and lysed for 10 min at 4 °C in 1 mL Cell Lysis Buffer (20 mM Tris-HCl (pH 8.0), 85 mM KCl, 0.5% NP-40) supplemented with EDTA-free protease inhibitor cocktail (Roche; 4693132001). The nuclei were collected by centrifugation at $500 \times g$ for 5 min at 4 °C and washed once in the same buffer. Nuclei were resuspended in 500 μL Nuclei Lysis Buffer (10 mM Tris-HCl (pH 7.5), 1% NP-40, 0.5% sodium deoxycholate, 0.1% SDS, protease inhibitor cocktail) and incubated for 10 min at 4 °C. Chromatin was fragmented by sonication 3×10 s at 60% duty cycle, with 30 s on wet-ice between sonication cycles, using a microtip-equipped SLPe sonifier (Branson Ultrasonics ™ Sonifier™, Brookfield, USA). The sonicated samples were centrifuged at $16,000 \times g$ for 10 min. The supernatants were collected and 50 μL (1/10) was set aside as input controls. The rest (450 μL) was diluted with 1500 μl ChIP Dilution Buffer (0.01% SDS, 1.2 mM EDTA, 1.1% Triton X-100, 16.7 mM Tris-HCl (pH 8), 167 mM NaCl) supplemented with protease inhibitors and mixed with 50 μL Dynabeads™ Protein G (Invitrogen; 10009D) coupled either to 3 μg anti-HA antibody (Invitrogen; MA5-27915) in case of HA-Smc6 analysis, 5 μg anti-RPB1 (8WG16) (Covance; MMS-126R) for RNA pol II, 2 μg anti-H3pan (Diagenode; C15410324) or 4 μg anti-H3.3 (Diagenode; C15210011). After overnight incubation at 4 °C on a rotating wheel, the beads were washed twice with 1 mL Cell Lysis Buffer, twice with high-salt buffer (50 mM HEPES-KOH (pH 7.5), 500 mM NaCl, 1 mM EDTA, 1% Triton X-100, 0.1% sodium deoxycholate), once with LiCl buffer (10 mM Tris-HCl (pH 8.0), 1 mM EDTA, 250 mM LiCl, 1% NP-40, and 1% sodium deoxycholate) and once with TE buffer (10 mM Tris-HCl (pH 8.0), 1 mM EDTA). To elute immunoprecipitated chromatin fragments, beads were incubated for 10 min at 65 °C in 400 μL freshly prepared elution buffer (1% SDS, 0.1 M NaHCO₃). DNA crosslinks were reversed by overnight incubation at 65 °C with 0.6 M NaCl and 80 μg proteinase K (Eurobio Scientific; GEXPRK01-I5). Samples were extracted once with Phenol−chloroform−isoamyl alcohol (Sigma; 77617), once with chloroform (Reactolab SA; P02410E16), ethanol precipitated and then resuspended in water. The input DNA samples were treated identically. The recovered DNA were quantified by real-time PCR using the KAPA SYBR FAST qPCR Kit Master Mix (2X) Universal (Roche; SFUKB) and the Bio-Rad CFX96 Real-time PCR System. The values shown in the figures are the ratios between the ChIP signals and the respective input DNA signals. The oligonucleotide primers used are listed in Supplementary Table 1.

ChIP-seq
ChIP-Seq DNA was purified as it was described in ChIP and Quantitative PCR paragraph. ChIP-seq were performed in biological monoplicat. ChIP-enriched DNA were used to prepare libraries and processed with the Illumina TruSeq ChIP kit according to manufacturer specifications. Library molarity and quality were assessed with the Qubit (Thermo-fisher Scientific) and Tapestation (Agilent Technologies−DNA High
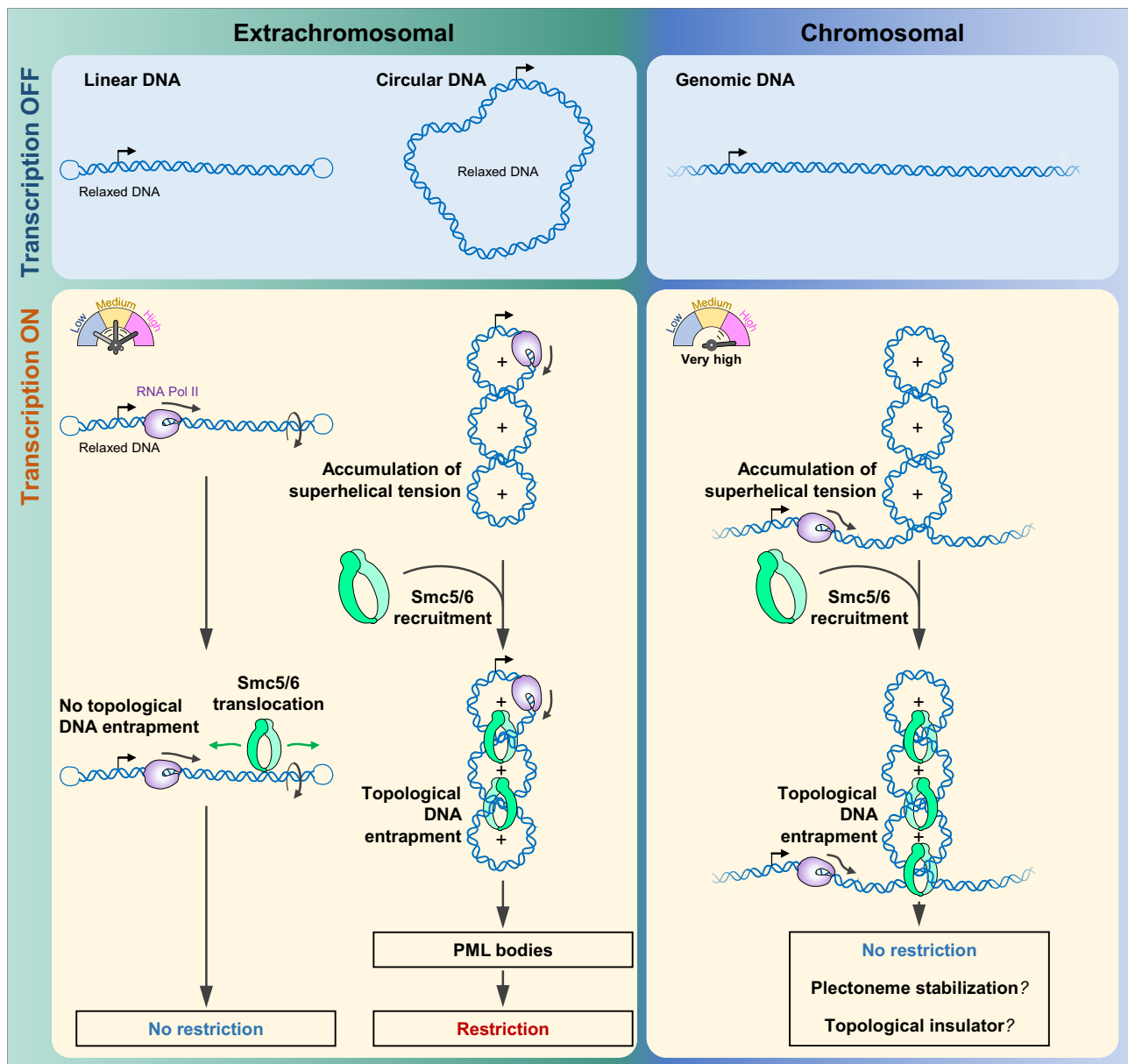
Fig. 7 | Speculative model. Upon transcription, the superhelical tension generated by the transcribing RNA polymerase II will be more significant on a covalently closed circular DNA molecule compared to a linear one, independently of the promoter strength. This will lead to the recruitment of Smc5/6 and to the topological DNA entrapment of the circular DNA while the complex will translocate along the linear DNA. On the chromosomes, an equivalent amount of superhelical tension can only be reached under conditions of a high transcriptional output, which also results in Smc5/6 recruitment. Based on previously reported data[25,26], we hypothesize that, on chromosomes upon DNA entrapment, Smc5/6 stabilizes the plectonemic DNA structures formed. By preventing supercoil spreading, Smc5/6 would therefore act as a topological insulator and/or facilitate the resolution of such DNA structures. The same DNA entrapment on extrachromosomal circular DNA leads to ecDNA recruitment to PML bodies and restriction[24].

sensitivity chip). Libraries were sequenced on a HiSeq 4000 and a NovaSeq 6000 Illumina sequencers for SR100 reads. Bioinformatics processing: sequenced reads were aligned to the human genome (build GRCh38.p13 downloaded from ENCODE) augmented with GLuc_episomal DNA sequence. We used the "mem" command of the software BWA (v0.7.17) for the alignment [BWA][63], and convert the output into sorted BAM with SAMTOOLS v1.10. ChIP-seq peak calling was performed with MACS2 (v2.2.7.1)[64] command "callpeak" and parameters "--format BAM --gsize hs --SPMR --keep-dup 1 --qvalue 0.05 --nomodel --extsize 1000" [MACS]. MACS2 is employed to identify peaks of HA-Smc5/6 by comparing DMSO or TPT conditions to the No HA reference condition, to detect RNA pol II peaks by comparing DMSO or TPT conditions to the Input (NT) condition, and to detect GapR-HA peaks by comparing GapR Low or GapR High conditions to the No HA reference condition.

Coverage computations and visualizations were done using scripts in R programming language making use of Bioconductor package. The code consisted in loading Smc5/6 peaks detection of MACS2 and retain those with a q-value ≤ 0.05 and a fold enrichment ≥ 2.5. Smc5/6 peaks were annotated with genes (taken from GENECODE v41 GTF) located within a 10 kb region of the peaks and curated manually. GenomicRanges R package and findOverlaps() method is used in this process. Then, Smc5/6 peaks and RNA pol II peaks were merged and reduced (R method GenomicRanges::reduce()) to determine genomic regions where they overlap (findOverlaps()). The ChIP-Seq alignment results of GapR (Low or High) were then juxtaposed

with previously identified Smc5/6 and RNA pol II peaks. GapR peaks detected using MACS2 with a q-value ≤ 0.05 and a fold enrichment ≥1.5 were also indicated.

Transcriptomic expression for RPE1 cell line was retrieved from GSE89413[46], and we consider FPKM normalized values of each gene to sort them by expression. We matched genes with Smc5/6 peaks by names.

To produce the heatmaps, we resized the ChIP-Seq mapped reads to 1 kb length, and compute at each genomic position the amount of overlap between forward-stranded and reverse-stranded reads (=2.min(fwd,rev)) normalized as read-per-million. A similar scaling factor is then applied to each gene of all condition so gene profiles can be compared from one gene to the other.

DNA extraction and qPCR
Cells were lysed in DNA lysis buffer (100 mM Tris-HCl (pH 7.5), 10 mM EDTA, 1% SDS) and briefly sonicated. Samples were extracted once with Phenol−chloroform−isoamyl alcohol (Sigma; 77617), once with chloroform (Reactolab SA; P02410E16), ethanol precipitated and then resuspended in water. The recovered DNA were quantified by real-time PCR using the KAPA SYBR FAST qPCR Kit Master Mix (2X) Universal (Roche; SFUKB) and the Bio-Rad CFX96 Real-time PCR System. The oligonucleotide primers used are listed in Supplementary Table 1.

EU labelling
Transcription inhibition was monitored through EU incorporation into nascent RNAs using Click-iT RNA Alexa Fluor 488 Imaging Kit (Invitrogen; C10329) according to the manufacturer's instructions. Briefly, after treatment as indicated in figure legends, hTERT-RPE1 cells seeded onto glass coverslips were incubated with 1 mM EU for 1 h. The cells were fixed with 3.7% formaldehyde in PBS for 15 min at RT and then permeabilized with 0.5% Triton X-100 for 15 min at RT. Incorporated EU was labeled by Click-iT reaction according to the manufacturer's instructions for 30 min at RT. The cells were washed with PBS before mounting the coverslips with VECTASHIELD containing DAPI (Vector Laboratories, H-1200). Immunofluorescence images were acquired on an Olympus DeltaVision wide-field microscope (GE Healthcare) equipped with a DAPI/FITC/TRITC/Cy5 filter set (Chroma Technology Corp.) and a Coolsnap HQ2 CCD camera (Roper Scientific) running Softworx 6.5.2 (GE Healthcare). 3D images were deconvolved using Softworx 6.5.2 (GE Healthcare). Fixed cells were imaged with a 40× NA 1.35 oil objective in 0.2 μm Z-stacks.

Live-cell imaging and immunofluorescence
For live-cell imaging of the hTERT-RPE1 cells containing the genomic excisable construct [GLuc^{circle}], cells were seeded in a glass bottom height-well μ-Slide Ibidi chamber (Ibidi; 80826) and co-transduced with lentiviruses containing either no gene insert (Mock) or HBx, plus or minus the Cre recombinase for 48 h. 4 h prior live-cell imaging, the culture medium was replaced by Leibovitz L-15 medium (ThermoFisher; 21083) supplemented with 10% FBS and 1% penicillin/streptomycin and containing 25 nM SiR-DNA (Spirochrome; SC007). Cells were acquired on a Nikon Eclipse Ti-E wide-field microscope (Nikon) equipped with a DAPI/FITC/Rhod/CY5 filter set (Chroma Technology Corp.), an Orca Flash 4.0 CMOS camera (Hamamatsu), and an environmental chamber using NIS software (Nikon). Z-stacks were imaged with z-slices separated by 2.5 μm, with 50 ms exposure per z-slice in the GFP and Cy5 channels using a 40× NA 1.3 oil objective and 2 × 2 binning.

For fixed-cell imaging, hTERT-RPE1 cells over-expressing HA-tagged version of Smc6 and either T7 RNA pol or Myc-NLS-vTop1B or hTERT-RPE1 cells expressing GapR-3xHA were grown onto acid-etched glass coverslips. Cells were fixed with 3.7% formaldehyde for 15 min before permeabilization with 0.5% Triton X-100 for 15 min followed by blocking for 1 h in PBS supplemented with 3% BSA. The final dilution of primary antibodies was 1:100 for anti-T7 RNA Polymerase (Creative

Diagnostics; CABT-B8990), 1:10 for anti Myc-Tag (DSHB; 9E 10) and the anti-HA (Invitrogen; MA5-27915) was used at 2 μg/mL. Secondary antibody conjugated with Alexa Fluor 488 either goat anti-rabbit IgG (Invitrogen; A-11008) or Alexa Fluor 488 donkey anti-mouse IgG (Invitrogen; A21202) were used at 1:400. All antibodies were diluted in PBS supplemented with 3% BSA. Primary and secondary antibodies were applied for overnight and 60 min, respectively. Immunolabelled cells were washed with PBS before mounting the coverslips with VECTASHIELD containing DAPI (Vector Laboratories; H-1200). Immunofluorescence images were acquired on an Olympus DeltaVision wide-field microscope (GE Healthcare) equipped with a DAPI/FITC/TRITC/Cy5 filter set (Chroma Technology Corp.) and a Coolsnap HQ2 CCD camera (Roper Scientific) running Softworx 6.5.2 (GE Healthcare). 3D images were deconvolved using Softworx 6.5.2 (GE Healthcare). Fixed cells were imaged with a 40× NA 1.35 oil objective in 0.2 μm Z-stacks. Alternatively, fixed cells expressing Myc-NLS-vTop1B were visualized with a Plan Apo 40x (NA 1.3 Oil DICIII) objective in 0.2 μm Z-stacks on a spinning disk microscope (Nipkow Disk) Zeiss Cell Observer.Z1 equipped with a HXP120 fluorescence wide-field visualization lamp and with a CSU X1 automatic Yokogawa spinning disk head. 512 × 512 pixel images were acquired with an Evolve EM512 camera and Visiview 4.00.10.

Two-dimensional agarose gel electrophoresis and Southern blot for DNA topological analysis
Extrachromosomal DNAs were extracted from ~40 × 10⁶ hTERT-RPE1 cells containing the genomic excisable [Gluc^{circle}] construct co-transduced with lentiviruses expressing the Cre Recombinase for 48 h. To enrich for ecDNA, DNA was prepared using the PureLink™ HiPure Plasmid Midiprep (ThermoFisher; K2100-05). Cells were resuspended in 15 mL of Resuspension Buffer (R3) and lysed in 15 mL of Lysis Buffer (L7) before precipitation in 15 mL of Precipitation Buffer (N3). After centrifugation for 10 min at >12,000 × g the supernatant was directly precipitated with isopropanol and centrifuged at 18,000 × g for 1 h at 4 °C. The pellet was washed in 70% ethanol before resuspension. As control, comparable negatively supercoiled circles with sequences identical to the ecDNA circles recovered from the cells were prepared in vitro using the Cre Recombinase (New England Biolabs; M0298S). Briefly, 250 ng of the plasmid used to generate the cell line with the excisable chromosomal reporter construct was incubated with Cre for 30 min at 37 °C. The reaction was terminated by heating at 70 °C for 10 min. For two-dimensional gel electrophoresis, we used 1.4% (w/v) agarose gel in TBE buffer (90 mM Tris-borate, 2 mM EDTA), gel migration was performed at 2 V/cm at 4 °C in a cold room using recirculating buffer for 2 × 24 h. The first-dimension electrophoresis was carried out in absence of intercalating agent. The second dimension was carried out at a 90° angle with respect to the first dimension with or without a 2 h soaking in chloroquine 7.8 μg/ml (Sigma; C6628). Second-dimension electrophoresis was performed in TBE buffer supplemented or not with chloroquine (7.8 μg/ml). After electrophoresis the gels were washed twice for 15 min in 0.125 M HCl, rinsed for 5 min in water, and washed for 30 min in transfer buffer (0.4 M NaOH containing 0.6 M NaCl). The DNA was transferred onto Hybond-N+ membrane (Amersham™ Hybond™-N+; RPN303B) in transfer buffer for 16 h and neutralized 15 min in 0.5 M Tris-HCl (pH 7.0), 1 M NaCl, before UV crosslinking at 1200 μJoules (x100) (standard auto-crosslink setting) using the Stratalinker (Stratagene UV 1800). The membrane was pre-hybridized (5 X Denhardt's, 45 mM Tris-HCl, pH 7.5, 1 mM EDTA, 1 M NaCl, 10% Dextran sulfate 500, 1% SDS and 100 μg/ml salmon sperm DNA) at 65 °C in hybridization oven (Big S.H.O.T III™ Hybridization Oven; Boekel Scientific) for a minimum of 3 hrs. Hybridization was performed at 65 °C for 16 h in fresh hybridization buffer containing the G-50 purified random-primed [α-³²P]dATP probe (Supplementary Table 3) labeled with the DecaLabel DNA Labeling Kit (ThermoFisher; K0622). After hybridization, the membranes were washed at 65 °C three times for 5 min in 2× SSC and 0.1% SDS and twice

for 15 min in 0.1× SSC and 0.1% SDS. The membranes were directly exposed to a Fuji BAS-IP MS 2040 E imaging plate (Cytivia; 28-9564-74) and the images were acquired on a Typhoon™ FLA 7000 biomolecular imager (Cytiva; 28-9558-09).

Statistics & reproducibility

The statistical analysis was performed using GraphPad Prism 8 (GraphPad). The statistical tests employed are described in the figure legends. Minimum of three independent biological replicates were performed in all experiments. Exception for ChIP-seq presented in Figs. 5 and 6 (N = 1). All Western blot images are representative of two biological repeats. No statistical method was used to predetermine sample size. No data were excluded from the analyses; the experiments were not randomized; the investigators were not blinded to allocation during experiments and outcome assessment.

Reporting summary

Further information on research design is available in the Nature Portfolio Reporting Summary linked to this article.

Data availability

All deep sequencing data used in this study are available in the GEO database under their respective accession code ChIP-Seq for HA-Smc6, RPB1, and GapR-HA [GSE231328], the ChIP-Seq data for Top1 [GSE212468], Top2 [GSE136943] and RNA-seq [GSE89413]. Any additional information required to reanalyze the data reported in this paper is available from the lead contact upon reasonable request. Source data are provided with this paper.

Code availability

This paper does not report original code since it is based on implementation of publicly available software.

References

1. Jeppsson, K., Kanno, T., Shirahige, K. & Sjögren, C. The maintenance of chromosome structure: positioning and functioning of SMC complexes. *Nat. Rev. Mol. Cell Biol.* **15**, 601–614 (2014).
2. Hassler, M., Shaltiel, I. A. & Haering, C. H. Towards a unified model of SMC complex function. *Curr. Biol.* **28**, R1266–R1281 (2018).
3. Adamus, M. et al. Molecular insights into the architecture of the human SMC5/6 complex. *J. Mol. Biol.* **432**, 3820–3837 (2020).
4. Aragón, L. The Smc5/6 complex: new and old functions of the enigmatic long-distance relative. *Annu. Rev. Genet.* **52**, 89–107 (2018).
5. Roy, S., Adhikary, H. & D'Amours, D. The SMC5/6 complex: folding chromosomes back into shape when genomes take a break. *Nucleic Acids Res.* **52**, 2112–2129 (2024).
6. Irmisch, A., Ampatzidou, E., Mizuno, K., O'Connell, M. J. & Murray, J. M. Smc5/6 maintains stalled replication forks in a recombination-competent conformation. *EMBO J.* **28**, 144–155 (2009).
7. Zhao, X. & Blobel, G. A SUMO ligase is part of a nuclear multiprotein complex that affects DNA repair and chromosomal organization. *Proc. Natl Acad. Sci.* **102**, 4777–4782 (2005).
8. Andrews, E. A. et al. Nse2, a component of the Smc5-6 complex, Is a SUMO ligase required for the response to DNA damage. *Mol. Cell. Biol.* **25**, 185–196 (2005).
9. Bermúdez-López, M. et al. ATPase-dependent control of the Mms21 SUMO ligase during DNA repair. *PLoS Biol.* **13**, e1002089 (2015).
10. Fousteri, M. I. & Lehmann, A. R. A novel SMC protein complex in Schizosaccharomyces pombe contains the Rad18 DNA repair protein. *EMBO J.* **19**, 1691–1702 (2000).
11. Potts, P. R. & Yu, H. The SMC5/6 complex maintains telomere length in ALT cancer cells through SUMOylation of telomere-binding proteins. *Nat. Struct. Mol. Biol.* **14**, 581–590 (2007).
12. Potts, P. R., Porteus, M. H. & Yu, H. Human SMC5/6 complex promotes sister chromatid homologous recombination by recruiting
13. De Piccoli, G. et al. Smc5–Smc6 mediate DNA double-strand-break repair by promoting sister-chromatid recombination. *Nat. Cell Biol.* **8**, 1032–1034 (2006).
14. Decorsière, A. et al. Hepatitis B virus X protein identifies the Smc5/6 complex as a host restriction factor. *Nature* **531**, 386–389 (2016).
15. Murphy, C. M. et al. Hepatitis B virus X protein promotes degradation of SMC5/6 to enhance HBV replication. *Cell Rep.* **16**, 2846–2854 (2016).
16. Bentley, P., Tan, M. J. A., McBride, A. A., White, E. A. & Howley, P. M. The SMC5/6 complex interacts with the papillomavirus E2 protein and influences maintenance of viral episomal DNA. *J. Virol.* **92**, e00356–18 (2018).
17. Gibson, R. T. & Androphy, E. J. The SMC5/6 complex represses the replicative program of high-risk human papillomavirus type 31. *Pathogens* **9**, 786 (2020).
18. Xu, W. et al. PJA1 coordinates with the SMC5/6 complex to restrict DNA viruses and episomal genes in an interferon-independent manner. *J. Virol.* **92**, e00825–18 (2018).
19. Han, C. et al. KSHV RTA antagonizes SMC5/6 complex-induced viral chromatin compaction by hijacking the ubiquitin-proteasome system. *PLoS Pathog.* **18**, e1010744 (2022).
20. Dupont, L. et al. The SMC5/6 complex compacts and silences unintegrated HIV-1 DNA and is antagonized by Vpr. *Cell Host Microbe* **29**, 792–805.e6 (2021).
21. Yiu, S. P. T., Guo, R., Zerbe, C., Weekes, M. P. & Gewurz, B. E. Epstein-Barr virus BNRF1 destabilizes SMC5/6 cohesin complexes to evade its restriction of replication compartments. *Cell Rep.* **38**, 110411 (2022).
22. Oravcová, M. et al. The Nse5/6-like SIMC1-SLF2 complex localizes SMC5/6 to viral replication centers. *eLife* **11**, e79676 (2022).
23. van Breugel, P. C. et al. Hepatitis B virus X protein stimulates gene expression selectively from extrachromosomal DNA templates. *Hepatology* **56**, 2116–2124 (2012).
24. Abdul, F. et al. Smc5/6 silences episomal transcription by a three-step function. *Nat. Struct. Mol. Biol.* **29**, 922–931 (2022).
25. Gutierrez-Escribano, P. et al. Purified Smc5/6 complex exhibits DNA substrate recognition and compaction. *Mol. Cell* **80**, 1039–1054.e6 (2020).
26. Serrano, D. et al. The Smc5/6 core complex is a structure-specific DNA binding and compacting machine. *Mol. Cell* **80**, 1025–1038.e5 (2020).
27. Pommier, Y., Nussenzweig, A., Takeda, S. & Austin, C. Human topoisomerases and their roles in genome stability and organization. *Nat. Rev. Mol. Cell Biol.* **23**, 407–427 (2022).
28. Jeppsson, K. et al. The chromosomal association of the Smc5/6 complex depends on cohesion and predicts the level of sister chromatid entanglement. *PLoS Genet* **10**, e1004680 (2014).
29. Silver, D. P. & Livingston, D. M. Self-excising retroviral vectors encoding the Cre recombinase overcome Cre-mediated cellular toxicity. *Mol. Cell* **8**, 233–243 (2001).
30. Kanno, T., Berta, D. G. & Sjögren, C. The Smc5/6 complex is an ATP-dependent intermolecular DNA linker. *Cell Rep.* **12**, 1471–1482 (2015).
31. Godiska, R. et al. Linear plasmid vector for cloning of repetitive or unstable sequences in Escherichia coli. *Nucleic Acids Res.* **38**, e88 (2010).
32. Kegel, A. et al. Chromosome length influences replication-induced topological stress. *Nature* **471**, 392–396 (2011).
33. Sobell, H. M. Actinomycin and DNA transcription. *Proc. Natl Acad. Sci.* **82**, 5328–5331 (1985).
34. Titov, D. V. et al. XPB, a subunit of TFIIH, is a target of the natural product triptolide. *Nat. Chem. Biol.* **7**, 182–188 (2011).
35. Jao, C. Y. & Salic, A. Exploring RNA transcription and turnover in vivo by using click chemistry. *Proc. Natl Acad. Sci.* **105**, 15779–15784 (2008).

36. Sandig, V., Lieber, A., Bähring, S. & Strauss, M. A phage T7 class-III promoter functions as a polymerase II promoter in mammalian cells. *Gene* **131**, 255–259 (1993).

37. Gothe, H. J. et al. Spatial chromosome folding and active transcription drive DNA fragility and formation of oncogenic MLL translocations. *Mol. Cell* **75**, 267–283.e12 (2019).

38. Canela, A. et al. Genome organization drives chromosome fragility. *Cell* **170**, 507–521.e18 (2017).

39. Das, S. K. et al. MYC assembles and stimulates topoisomerases 1 and 2 in a "topoisome". *Mol. Cell* **82**, 140–158.e12 (2022).

40. Shuman, S. Site-specific DNA cleavage by vaccinia virus DNA topoisomerase I. Role of nucleotide sequence and DNA secondary structure. *J. Biol. Chem.* **266**, 1796–1803 (1991).

41. Fernandez-Beros, M.-E. & Tse-Dinh, Y.-C. Vaccinia virus DNA topoisomerase I preferentially removes positive supercoils from DNA. *FEBS Lett.* **384**, 265–268 (1996).

42. Menolfi, D., Delamarre, A., Lengronne, A., Pasero, P. & Branzei, D. Essential roles of the Smc5/6 complex in replication through natural pausing sites and endogenous DNA damage tolerance. *Mol. Cell* **60**, 835–846 (2015).

43. Mahrik, L. et al. The SAGA histone acetyltransferase module targets SMC5/6 to specific genes. *Epigenetics Chromatin* **16**, 6 (2023).

44. Barlow, J. H. et al. Identification of early replicating fragile sites that contribute to genome instability. *Cell* **152**, 620–632 (2013).

45. Eick, D. & Geyer, M. The RNA polymerase II carboxy-terminal domain (CTD) code. *Chem. Rev.* **113**, 8456–8490 (2013).

46. Harenza, J. L. et al. Transcriptomic profiling of 39 commonly-used neuroblastoma cell lines. *Sci. Data* **4**, 170033 (2017).

47. Meroni, A. et al. NEDDylated cullin 3 mediates the adaptive response to topoisomerase 1 inhibitors. *Sci. Adv.* **8**, eabq0648 (2022).

48. Gittens, W. H. et al. A nucleotide resolution map of Top2-linked DNA breaks in the yeast and human genome. *Nat. Commun.* **10**, 4846 (2019).

49. Gibson, E. G., Oviatt, A. A. & Osheroff, N. Two-dimensional gel electrophoresis to resolve DNA topoisomers. in *DNA Electrophoresis: Methods and Protocols* (ed. Hanada, K.) 15–24 (Springer US, New York, NY, 2020). https://doi.org/10.1007/978-1-0716-0323-9_2.

50. Shure, M., Pulleyblank, D. E. & Vinograd, J. The problems of eukaryotic and prokaryotic DNA packaging and in vivo conformation posed by superhelix density heterogeneity. *Nucleic Acids Res.* **4**, 1183–1206 (1977).

51. Abremski, K., Frommer, B. & Hoess, R. H. Linking-number changes in the DNA substrate during Cre-mediated *loxP* site-specific recombination. *J. Mol. Biol.* **192**, 17–26 (1986).

52. Guo, M. S., Haakonsen, D. L., Zeng, W., Schumacher, M. A. & Laub, M. T. A bacterial chromosome structuring protein binds overtwisted DNA to stimulate Type II topoisomerases and enable DNA replication. *Cell* **175**, 583–597.e23 (2018).

53. Guo, M. S., Kawamura, R., Littlehale, M. L., Marko, J. F. & Laub, M. T. High-resolution, genome-wide mapping of positive supercoiling in chromosomes. *eLife* **10**, e67236 (2021).

54. Taschner, M. et al. Nse5/6 inhibits the Smc5/6 ATPase and modulates DNA substrate binding. *EMBO J.* **40**, e107807 (2021).

55. Keszthelyi, A., Minchell, N. E. & Baxter, J. The causes and consequences of topological stress during DNA replication. *Genes* **7**, 134 (2016).

56. Ma, J. & Wang, M. D. DNA supercoiling during transcription. *Biophys. Rev.* **8**, 75–87 (2016).

57. Liu, L. F. & Wang, J. C. Supercoiling of the DNA template during transcription. *Proc. Natl Acad. Sci.* **84**, 7024–7027 (1987).

58. Jeppsson, K. et al. Loop-extruding Smc5/6 organizes transcription-induced positive DNA supercoils. *Mol. Cell* **84**, 867–882.e5 (2024).

59. Janissen, R. et al. All eukaryotic SMC proteins induce a twist of -0.6 at each DNA-loop-extrusion step. Preprint at https://doi.org/10.1101/2024.03.22.586328 (2024).

60. Davidson, I. F. et al. Cohesin supercoils DNA during loop extrusion. Preprint at https://doi.org/10.1101/2024.03.22.586228 (2024).

61. Niu, C. et al. The Smc5/6 complex restricts HBV when localized to ND10 without inducing an innate immune response and is counteracted by the HBV X protein shortly after infection. *PLoS ONE* **12**, e0169648 (2017).

62. Mordstein, C. et al. Transcription, mRNA export, and immune evasion shape the codon usage of viruses. *Genome Biol. Evol.* **13**, evab106 (2021).

63. Li, H. Aligning sequence reads, clone sequences and assembly contigs with BWA-MEM. Preprint at http://arxiv.org/abs/1303.3997 (2013).

64. Zhang, Y. et al. Model-based analysis of ChIP-Seq (MACS). *Genome Biol.* **9**, R137 (2008).

Acknowledgements

Author contributions

Conceptualization of the project A.D. and M.S. A.D. designed and carried out all the experiments. A.D. G.P. and J.P. analyzed and interpreted the ChIP-Seq data. C.C. acquired and analyzed all the microscopy data. B.B. performed the western blots shown in Figs. 3C, D, 4F and S4A. M.S. acquired the funding. A.D. and M.S. analyzed the data. A.D. wrote the manuscript with input from all authors.

Competing interests

The authors declare no competing interests.

Additional information

Supplementary information The online version contains supplementary material available at https://doi.org/10.1038/s41467-024-50646-w.

Correspondence and requests for materials should be addressed to Aurélie Diman.

Peer review information *Nature Communications* thanks the anonymous reviewers for their contribution to the peer review of this work. A peer review file is available.

Reprints and permissions information is available at http://www.nature.com/reprints

Publisher's note Springer Nature remains neutral with regard to jurisdictional claims in published maps and institutional affiliations.